The Elasticity of Single Titin Molecules Using a Two-Bead Optical Tweezers Assay

Mark C. Leake,† David Wilson,* Mathias Gautel,‡ and Robert M. Simmons*
*Medical Research Council Muscle and Cell Motility Unit, †Randall Centre for Molecular Mechanisms of Cell Function, King's College London, London SE1 1UL, United Kingdom; and ‡Department of Physical Biochemistry, Max-Planck-Institut für molekulare Physiologie, 44202 Dortmund, Germany

ABSTRACT Titin is responsible for the passive elasticity of the muscle sarcomere. The mechanical properties of skeletal and cardiac muscle titin were characterized in single molecules using a novel dual optical tweezers assay. Antibody pairs were attached to beads and used to select the whole molecule, I-band, A-band, a tandem-immunoglobulin (Ig) segment, and the PEVK region. A construct from the PEVK region expressing >25% of the full-length skeletal muscle isoform was chemically conjugated to beads and similarly characterized. By elucidating the elasticity of the different regions, we showed directly for the first time, to our knowledge, that two entropic components act in series in the skeletal muscle titin I-band (confirming previous speculations), one associated with tandem-immunoglobulin domains and the other with the PEVK region, with persistence lengths of 2.9 nm and 0.76 nm, respectively (150 mM ionic strength, 22°C). Novel findings were: the persistence length of the PEVK component rose (0.4–2.7 nm) with an increase in ionic strength (15–300 mM) and fell (3.0–0.3 nm) with a temperature increase (10–60°C); stress-relaxation in 10–12-nm steps was observed in the PEVK construct and hysteresis in the native PEVK region. The region may not be a pure random coil, as previously thought, but contains structured elements, possibly with hydrophobic interactions.

INTRODUCTION

The giant muscle protein titin (connectin), molecular mass ~3 MDa (Wang et al., 1979), is responsible for the major part of the passive elasticity of vertebrate muscle (Wang and Greaser, 1985; Trombitas et al., 1991; Granzier and Irving, 1995). It extends across the entire half-sarcomere from the Z-disk at its N-terminus to the M-line at its C-terminus. Under normal conditions the A-band region is firmly associated with the myosin thick filament and is considered to be inextensible, but the I-band section is free to elongate and therefore constitutes the physiologically relevant portion (Fürst et al., 1988; Whiting et al., 1989; Trombitas et al., 1991).

In recent years, the mechanical characteristics of titin have been determined in a number of preparations: in myofibrils or single cells, where most of the elasticity derives from titin and in which fluorescence-labeled or gold-labeled antibodies to specific titin epitopes have been used to apportion stretch between different regions of the molecule (Trombitas et al., 1993; Linke et al., 1996, 1998a; Gautel and Goulding, 1996; Gautel et al., 1996a; Granzier et al., 1996), and in single molecules or expressed fragments, using optical tweezers or atomic force microscopy (AFM) techniques (Kellermayer et al., 1997; Rief et al., 1997; Tskhovrebova et al., 1997). Measurements relating to polymer properties are also available from light scattering measurements (Higuchi et al., 1993), NMR (Fraternali and Pastore, 1999), and electron microscopy (EM) (Tskhovrebova and Trinick, 2001).

The I-band region of skeletal muscle titin has a sequence consisting mainly of 43–96 immunoglobulin (Ig) domains (Labeit et al., 1992; Labeit and Kolmerer, 1995) and a specialized elastic PEVK region, so-called because it is rich in proline, glutamate, valine, and lysine residues. At a low force, the main contribution to the compliance of titin comes from the nonlinear, entropic elasticity of the random chain of Ig domains (Tskhovrebova et al., 1997; Linke et al., 1998b). As the molecule is stretched the end-to-end distance increases as the chain is straightened, and force rises. At greater stretch, the Ig chain becomes stiffer and the PEVK region then contributes more to compliance. In experiments on isolated whole titin molecules, the A-band region (composed mainly of 123 Ig and 48 Fn) domains also comes into play.

A third component of elasticity may be supplied by unfolded I-band Ig domains: these domains unfold upon stretch at a rate that depends on force and rate of stretch (Evans and Ritchie, 1999). Once unfolded, most domains do not refold until the force is reduced to near zero (Kellermayer et al., 1997; Rief et al., 1997; Tskhovrebova et al., 1997; Carrion-Vazquez et al., 1999). Unfolding appears to explain much of the stress relaxation shown by stretched passive muscle (Minajeva et al., 2001), but its exact role is unclear. Unfolding may constitute a mechanism for resetting stiffness

Submitted October 4, 2003, and accepted for publication May 3, 2004.

Address reprint requests to Robert M. Simmons, Randall Centre, King's College London, New Hunt's House, Guy's Campus, London SE1 1UL, UK. Tel.: 44-1672-562281; E-mail: robert.simmons@tiscali.co.uk.

Mark C. Leake's present address is Clarendon Laboratory, University of Oxford, Parks Road, Oxford, OX1 3PU, UK.

Mathias Gautel's present address is Randall Centre for Molecular Mechanisms of Cell Function, King's College London, New Hunt's House, Guy's Campus, London SE1 1UL, UK.

0006-3495/04/08/1112/24 $2.00

doi: 10.1529/biophysj.103.033571

when a muscle is extended to a new mean length (Tskhovrebova and Trinick, 2000); or it may provide a safety mechanism to prevent damage from a force overload (Rief et al., 1997;Tskhovrebova et al., 1997); or a fraction of the Ig domains may remain more or less permanently unfolded and contribute additional compliance (Kellermayer et al., 1997), though recent data suggests that the unfolding pathway of most titin I-band domains will not result in unfolding at physiological forces (Williams et al., 2003). These mechanisms are not mutually exclusive.

Two polymer models, the worm-like chain (WLC) and the freely jointed chain (FJC), can be used to describe these sources of elasticity. These random chain, entropic models are characterized by the extended length of the chain, the contour length (L_c), and the functional segment length, which is the persistence length (L_p) in the worm-like chain model and the Kühn length (L_k) in the freely jointed chain model. In principle, a multiple component polymer having serially distinct chains of different segment length can be characterized from mechanical measurements, provided the difference between the segment lengths is sufficiently great. Two types of elastic component have proved to be of interest: i), the chain of Ig (and Fn) domains, where structural NMR data (Fraternali and Pastore, 1999) have shown the length of a single Ig domain is ~4.5 nm. If the domains are linked in tandem via a universal joint with no steric hindrance then L_k should be ~4.5 nm and $L_p \sim 2.2$ nm; and ii), unfolded or random coil structures, where the minimal segment length is the extended residue repeat of 0.36 nm, where L_k should be ~0.36 nm and $L_p \sim 0.18$ nm, if there is no hindrance to rotation.

Tskhovrebova et al. (1997) fitted force-extension curves of the whole rabbit longissimus dorsi muscle titin molecule with a two-component polymer model. The components were identified with a chain comprising the PEVK region (here referred to as chain I) and the chain of Ig/Fn domains (chain II): for chain I, the value of L_p, 0.15 nm, was close to the value expected for a random, unhindered polypeptide chain, and the value of L_c, 416 nm, was close to the predicted extended length of the PEVK region. Similarly for chain II, L_p at 4.6 nm was close to the value expected from the repeat distance of Ig and Fn domains, and L_c at 1020 nm coincided with the value expected from sequence information for the total length of Ig/Fn domains.

For the whole molecule, fitted with a single component model, a further laser-tweezers study gave values of 1.5–2.0 nm (Kellermayer et al., 1997, 1998, both using rabbit longissimus dorsi muscle titin), consistent with the two-component fit by Tskhovrebova et al. (1997) in that a single component approximation to a two-component system will generate an effective persistence length that is a weighted average of the persistence lengths of the two-component system and thus a value intermediate between the two. However, a recent study on a cardiac muscle PEVK construct gave L_p values with a range from 0.4 to 2.5 nm (Li et al., 2002, using a concatemer of human cardiac PEVK and the human Ig domain I27, $(I27\text{-}PEVK)_3$), with a similar range of persistence lengths observed using recombinant soleus muscle PEVK molecules (Labeit et al., 2003), much higher than the estimate of Tskhovrebova et al. (1997) for the putative native PEVK domain, also to be compared with an estimate of 2.0 nm for the PEVK region from Trombitas et al. (1998) using human soleus muscle fibers. There is also the possibility that unfolded Ig domains contribute to the lower L_p component, but AFM mechanical studies have given L_p values of 0.4–0.8 nm or unfolded Ig/Fn domains either in whole titin or an expressed region containing tandem Ig repeats (Rief et al., 1997, using constructs of human I91–93 and I91–98; Rief et al., 1998, using constructs of human I91–98, I112–118, and A60–65; Carrion-Vazquez et al., 1999, using concatemers of I27, $(I27)_8$, and $(I27)_{12}$).

In addition, electron microscopy (Tskhovrebova and Trinick, 2001, using rabbit longissimus dorsi muscle titin) and dynamic light scattering (Higuchi et al., 1993, using rabbit longissimus dorsi muscle titin) of the whole molecule have suggested L_p values for the whole titin molecule of 13.5 and 15.0 nm, respectively, far greater than any of the other single molecule estimates, though consistent with an estimate of 15.0 nm for the tandem-Ig region from immunoelectron microscopy of stretched human soleus muscle fibers (Trombitas et al., 1998). Data from single myofibril stretches have also been fitted by a broad range of persistence lengths, typically with a mean of ~0.6 nm for the PEVK region, with the suggestion of an additional enthalpic component to the elasticity (Linke et al., 1998a, using rat psoas myofibrils) and as much as 42 nm for the tandem Ig region (Linke et al., 1998b, using rat psoas myofibrils).

One difficulty in obtaining clear results in mechanical studies is that, without special precautions, purified titin is likely to be a mixture of isoforms of different lengths and may also be multimeric (Tskhovrebova and Trinick, 1997, using rabbit longissimus dorsi muscle titin). There are several isoforms, generated from a series of exon-skipping events of a single gene (Freiburg et al., 2000). The full-length isoform is expressed in soleus and diaphragm, with the shortest isoform expressed in cardiac muscle that has 53 fewer IgI domains and a much shorter PEVK region of 186 residues compared to 2181 in soleus, accounting for its greater intrinsic stiffness. Oligomers of titin, with up to five chains connected, form the bulk of purified titin when it is eluted from a gel filtration column. The effect of multiple attachments in supposedly single molecule experiments is to give a low apparent value of L_p, and this could help to explain the low value for the PEVK domain obtained by Tskhovrebova et al. (1997).

Using an improved two-bead laser-tweezers method, we have reinvestigated the elastic properties of skeletal muscle titin, employing a range of antibodies raised against specific epitopes to attach beads to locations along the molecule. We used skeletal muscle titin purified from a single fast muscle

(longissimus dorsi) to restrict the number of isoforms present, and we used a fraction that was shown by EM to be almost exclusively monomeric. Using a protocol designed to reduce the number of multiple and nonspecific attachments, we derived polymer fits to force-extension curves for the whole molecule, the A-band region, the I-band region, and two subdivisions of the I-band, the PEVK region and a short tandem Ig region. Only in the I-band region and the whole molecule was it necessary to use a two-component model: chain I with a low value of L_p (0.5–0.8 nm) and chain II with a high value (3.0–3.6 nm). The tandem Ig/Fn regions (the A-band and tandem Ig region) and the PEVK region could each be fitted with a single component model, with L_p values similar to those found for chain I and chain II, respectively. In addition, chain I was not found in cardiac muscle titin, in which the PEVK region is greatly truncated. In the case of skeletal muscle titin, chain I is therefore very likely to derive from the (large) PEVK region.

The value of the short L_p component (chain I) depended on ionic strength, and we investigated this dependence more thoroughly together with the temperature dependence in the native PEVK region and in a construct comprising about one-quarter of the native PEVK sequence. Stepwise lengthening was detected with stretch, particularly with the PEVK construct, tentatively suggesting that there are regions in the PEVK domain corresponding to short structures that reversibly unfold and refold with stretch and release. These may correspond to the repeated charged regions of PEVK identified from the sequence (Greaser, 2001) and shown by NMR to have homology to a polyproline-II left-handed helix coil (Ma et al., 2001).

MATERIALS AND METHODS

Preparation of titin

Skeletal muscle titin was prepared from the longissimus dorsi muscle of New Zealand white rabbit, *Orycytolagus cuniculus*, using the method of Trinick et al. (1984) with minor modifications. At the end of the procedure, the crude extract of titin was pumped through a large pore gel filtration column (~5 cm diameter × 1 m length, Sepharose 4B-CL, Sigma-Aldrich, St. Louis, MO), collecting ~80 fractions of 4.0 ml, monitoring A_{280}. Low-angle rotary-shadowed specimens of various fractions dialysed into buffer E (Table 1), dried and viewed by electron microscopy, showed that the first titin fractions eluted were highly oligomeric in nature, consisting of perhaps as many as five monomers, decreasing to two with the peak of the A_{280} signal; subsequent fractions were found to be largely monomeric and uniform in terms of measured molecular contour length until later fractions where shorter components emerge. Titin remained stable for over 4 months when stored at −20°C in 50% glycerol.

Bovine cardiac muscle titin, prepared in a similar manner, was donated by Prof. John Trinick (Leeds University, UK).

PEVK construct preparation and sequence

A fragment of skeletal titin encompassing residues 5594–6143 of skeletal titin (European Molecular Biology Laboratory X90569, Heidelberg, Germany) was subcloned into a modified pET vector, introducing a C- and N-terminal cysteine, and referred to as PEVK1. PEVK1 was expressed in *Escherichia coli* at 15°C, purified by nickel-chelating chromatography by use of an N-terminal His^6-tag followed by anion-exchange chromatography on a monoQ column (Amersham-Pharmacia, Buckinghamshire, UK). The His^6-tag was cleaved off using TEV protease essentially as described (Young et al., 1998). The PEVK fragment was found to be stable at 4°C for several weeks in the presence of protease inhibitors (as above) and for several months at −20°C in 50% glycerol.

TABLE 1 List of buffers used in bead preparation and EM of titin fractions

	Contents
A	300 mM sodium chloride, 40 mM sodium borate, 4 mM sodium azide, pH 8.2
B	150 mM sodium chloride, 20 mM sodium phosphate, 4 mM sodium azide, pH 7.4
C	150 mM sodium chloride, 20 mM sodium phosphate, 5 mM EDTA, 4 mM azide, pH 7.2
D	200 mM Tris-HCl, pH 8.0
E	150 mM ammonium acetate, 20% (w/v) glycerol, pH 7.4
F	150 mM sodium chloride, 20 mM sodium phosphate, 0.05% (w/v) Tween-20, pH 7.4

Bead preparation for native titin

For native titin, several antibodies with well-defined epitopes, mostly sequence assigned, were used to cross-link the protein to latex beads, 2.0-μm diameter polystyrene beads derivatized with aldehyde-sulfate groups (Interfacial Dynamics, Portland, OR), using the method of Tskhovrebova et al. (1997) with minor modifications. If fluorescent beads were required, 1 μM rhodamine isothiocyanate (RITC) was incubated before the final wash and incubation with bovine serum albumin (BSA). Stored at 4°C, the antibody-labeled beads remained viable, in terms of ability to bind to titin, for 2–3 months. The binding of titin followed the method of Kellermayer et al. (1997). The surface density of titin could be controlled by varying the concentration in the incubation mixture.

Tethering via sulfo-SMCC

The titin construct, PEVK1, was engineered to have a free sulphydryl group on each terminus. The entire length of titin PEVK contains no cysteine residues, allowing therefore end-specific thiol-directed attachment. The terminal sulphydryl groups were used to tether to amine-coated polystyrene latex beads via the water-soluble maleimide *N*-hydroxy-succinimide heterobifunctional cross-linker, sulfo-succinimidyl 4-(*N*-maleimidomethyl) cyclohexane-1-carboxylate (Sulfo-SMCC; Pierce Chemical, Rockford, IL), to constrain the entire length of the construct between two beads.

The protocol used was modified from the method of the manufacturer (Pierce Chemical, ''Instructions: NHS-Esters Crosslinkers'', 9/1997). A quantity of 1.0 ml 0.5-mg/ml suspension of 2.1-μm diameter polystyrene latex beads derivatized with aliphatic amine groups (Interfacial Dynamics) was spun down and the pellet resuspended in 50 μl 1-mg/ml solution Sulfo-SMCC in buffer C, the incubation allowed to proceed for 1 h at room temperature (if fluorescent beads were required, 5 μl 1 μM RITC in buffer C was added and left to incubate for a further 5 min at room temperature), and 10 μl 200 mM buffer D was added to quench the NHS-ester conjugation, incubating for a further 5 min. The beads were then washed, spun down, and resuspended in 100 μl buffer B.

To coat the SMCC-beads in the construct, 100 μl beads were first spun down and the pellet resuspended in 50 μl 2-mM solution of β-mercaptoethanol, incubating for 30 min at room temperature to preblock ~80% of the active maleimide sites. The beads were then washed, spun down, and resuspended in 50 μl 0.2 nM PEVK1, incubating overnight on an

agitator at 4°C. After a final wash and spin, the beads were resuspended in 80 μl buffer C.

Immunofluorescence

Immunofluorescence studies on antititin antibodies were performed on single relaxed myofibrils prepared from rabbit longissimus dorsi muscle by a modification of a technique developed for rabbit psoas muscle (Linke et al., 1997). Photomicrographs taken under fluorescence and phase contrast were scanned, and image analysis was performed using the shareware package Scion Image. Intensity profiles were obtained across an 8–10 sarcomere length of myofibril mean averaging across a 20-pixel width at each point on the length axis. The profile corresponded to an equally spaced Gaussian intensity doublet across each Z-disk. The whole intensity profile was fitted with Gaussians using a least-squares routine written in Matlab to obtain the doublet separation. At separations of less than ~50 nm, two Gaussians could no longer be resolved.

The measured loci of the epitopes are listed in Table 2, and are shown in comparison to their positions predicted from the sequence for soleus muscle, supposing a titin molecule to be fully extended. In deriving the predicted values, it was assumed that the N-terminus of titin begins at the center of the Z-disk (Gautel et al., 1996b). Lengths were assumed as follows: 4.4 nm for IgI- and Fn3-like domains (Pfuhl et al., 1995), ~15 nm for each Z-repeat lattice spacing (Young et al., 1998), and 0.36 nm for individual amino acid residues in a random-coil configuration.

Measurement of surface density

The ratio of beads/antibodies in the incubation mixture gave a maximum of $\sim 6.4 \times 10^4$ antibodies and ~60 titin molecules per bead. The detection by ELISA of unbound anti-N2-A antibody remaining in the supernatant of the incubation mixture gave a value of $\sim 2.1 \times 10^4$ antibodies per bead. Using the same assay for titin, detecting both the unbound titin and bound titin after glycine dissociation, gave a value of 18–25 titin molecules per bead.

Surface plasmon resonance on a stationary phase of titin and a mobile phase of free-flowing anti-N2-A gave a spontaneous dissociation rate of 2.5×10^{-3} s^{-1}. Assuming a width of activation potential for the dissociation transition of 0.4 nm (Schwesinger et al., 2000) and modeling the most probable dissociation force by the formulation of Evans and Ritchie (1997) suggested a most likely force at which dissociation occurs of 80–95 pN for the rates of loading used in the dynamic stretch protocol (20–200 pN s^{-1}). This was in excess of the maximal force applied in the optical tweezers experiments.

Optical tweezers

The single bead technique used previously in this laboratory for full-length titin (Tskhovrebova et al., 1997) requires a very large geometric correction at the shorter lengths needed in this study; so instead we used a two-bead system (Leake et al., 2003), similar in approach to Kellermayer et al. (1997). In the bulk of the experiments a 2-W near infrared laser (Nd:YLF 1.047 μm TFR, Spectra Physics, Mountain View, CA) was used. Two independent single-beam gradient traps were used, similar to the design of Simmons et al. (1996) except where stated.

The objective was mounted on a piezoelectric transducer (PZT) focusing device (Physik Instrumente, Karlsruhe, Germany), which allowed submicron precision movement over a range of 0–0.35 mm. Movement of one trap (trap 1) was effected by a pair of acousto-optic modulators (AOM; Isle Optics, Taunton, UK), using negative feedback to act as a tensiometer (Simmons et al., 1996). The other trap (trap 2) was positioned by two galvanometer-driven mirrors (Cambridge Technology, Cambridge, MA). The galvanometer system was chosen as it provided the large extensions needed for the whole titin molecule experiments. The position of the two trapped beads was monitored by splitting and focusing the brightfield image onto two separate 1-mm diameter quadrant photodiode detectors, QD1 and QD2. The quadrant detectors had a bandwidth of ~15 kHz. The overlap between the images and also the overlap between the laser beams of the two beads had to be minimized. This was in part achieved by using 2-μm diameter beads, though corrections were necessary. Photodiode sensitivity was optimized by focusing the bead image to a dark outer ring with a lighter center, with the outer diameter of the dark ring roughly 20% larger than that of the quadrant detector.

Trap stiffness was routinely measured by a method utilizing Stokes' Law, which was found to be in satisfactory agreement with methods employing the measured Brownian motion of the trapped bead and the corner frequency of the power spectral density (Svoboda and Block, 1994).

The discrimination between bead types in these two-bead experiments was made possible by making one of the sets of beads fluorescent with RITC and observing the fluorescence image with a separate charge-coupled device (CCD) camera.

Formation of tethers

For most experiments, the beads were injected into a simple flow cell, constructed from a glass microscope slide and a glass coverslip, with a volume of ~35 μl. One bead was trapped in trap 1 (tensiometer), and the tether was stretched by moving trap 2 holding the other bead, similar to the protocol of Leake et al. (2003).

TABLE 2 Comparison of antibody positions from immunofluorescence (IF) of relaxed longissimus dorsi myofibrils with antigen positions from sequence

		Distance to Z-disk/nm		
Antibody	Epitope	IF	Sequence	Reference
T12	~I-band N-terminus	40 ± 15	60–100	Fürst et al. (1988)
Anti-N2-A*	I-band, Ig's I16–17	135 ± 40	125–400	Linke et al. (1996)
Anti-I84–86*	I-band, Ig's I84–86	430 ± 100	415	Linke et al. (1998b)
Anti-I105*	~A/I junction	510 ± 100	600	Bennett and Gautel (1996)
AB5	M-line	1020 ± 200	1180	Whiting et al. (1989)

Antibody positions are given as mean ± SD. Assumptions made in deriving values from sequence information: 1), The M-line is ~1300 nm from the center of the Z-disk (sarcomere length 2.6 μm). 2), The A-band region of the sequence does not extend, and thus the A/I junction is at ~700–800 nm from the M-line. 3), Between the A/I junction and the C-terminus of the PEVK region the Ig's are fully straightened, and each contribute 4.4 nm to the total distance from the Z-disk. 4), The N2-A epitope position is determined by counting back from the Z-disk, but since the number of differentially spliced Ig domains C-terminal to I15 has not yet been reported for rabbit longissimus dorsi muscle isoform, there is a large possible range from 0 (as in the cardiac muscle N2-B titin isoform) to 53 (as in the full-length soleus muscle titin isoform); these Ig's are fully straightened. 5), There is a range of 4–6 Z-repeats in the Z-disk with a lattice spacing of ~15 nm for each (Peckham et al., 1997; Young et al., 1998).
*Antibodies anti-N2-A, anti-I84–86, and anti-I105 were (pre-2001) designated N2-A, I20/22, and I41, respectively.

The best method for producing a tethered bead pair was to tap together heterogeneous pairs (Kellermayer et al., 1997). A low frequency triangle wave of typically 1 Hz was applied to the *x* axis galvanometer (where *x* is the direction along the axis between the beads), large enough for the beads to touch at maximal displacement of bead 2.

An advantage of this approach was that it directly generated a calibration function for QD2 in the presence of bead 1. At a small separation of the beads, the Airy disk of bead 1 was detected by QD2, resulting in an effective reduction of the sensitivity of QD2 to movements of bead 2 by as much as 30%; a calibration for QD2 in the presence of bead 1 was obtained for each bead pair studied, using a polynomial fit as for QD1. The response was linear for a bead separation of up to ~300 nm and had a practical range of ~600 nm. For greater separations, a larger split photodiode detector was employed. This had the disadvantage that sensitivity was ~fourfold lower, but the advantage that the correction needed for bead image overlap was negligible.

Depending upon the range of surface densities of titin and antibody (or PEVK construct and SMCC) employed, the time taken for tether formation could be as low as a few seconds and as high as 15 min. The likelihood of multiple tether formation is obviously higher the greater the surface density, and, as addressed later, a compromise value was chosen that would give a mean tether formation time of at least 5 min.

Sustained contact, where a bead pair is held in contact for anything from a few seconds to several minutes, and then pulled apart, was found to produce an unacceptably high proportion both of very stiffly tethered beads where a gap could still be discerned between the two, consistent with multiple tether formation, and of bead pairs where no gap could be observed even at the highest trapping forces achievable of ~150 pN, probably due to adhesion between the latex of the beads, despite blocking with bovine serum albumin.

Applied stretches

For triangle wave stretches, the molecule was extended at 1 Hz, starting with a small amplitude oscillation, usually less than 50 nm, and subsequently at increased stationary bead-bead separation by offsetting the *x* direction galvanometer (along the axis between the beads) until the beads just touched at the extremity of the oscillation as before. The highest force that could be obtained was 150 pN, but the practical limit was ~80 pN at which the position of the trapped beads became unstable.

For square wave stretches, bead 1 was held in a position feedback-clamp, and bead 2 oscillated with a square wave. The frequency was 0.05–5 Hz, and the amplitude was adjusted as for triangle waves.

Data acquisition and analysis

Data were acquired continuously at a sample rate of 1 kHz, with retrospective low-pass filtering using a first-order Butterworth filter with a frequency cutoff of 100 Hz. Force-extension data were fitted with both one- and multiorder-component freely jointed chain (Florey, 1969) and worm-like chain (Marko and Siggia, 1995) models, including the presence of enthalpic components and higher order improvements to the worm-like chain model, using routines written in Matlab that applied a Nelder-Mead downhill-simplex minimization algorithm (Nelder and Mead, 1965). Different models within each same data set were compared on a pairwise basis by applying a Student's *t*-test between each relevant goodness-of-fit factor to test if a statistically significant improvement in fitting had occurred at a confidence level of $P < 0.01$. The equations used and details of the fitting and statistical methods are given in the Supplementary Material.

Antibody experiments

In preliminary experiments, no marked differences were found depending on which one of a pair of antibody-labeled beads was precomplexed with titin or which bead of a pair was held in the fixed-position trap. The identical procedure was, however, followed for each bead pair within a set of experiments: the titin was always preincubated with the bead carrying the antibody to the epitope nearer to the M-line.

Tethers fell into two distinct populations: short-lived tethers (roughly two-thirds of the total number) that lasted for less than 10 stretch-release cycles before breaking and long-lived tethers that lasted for the duration of the stretch experiment (typically at least 5 min) without breaking.

The experiments were performed at room temperature, ~22°C, in a 10-mM HEPES buffer, pH 7.2, with total ionic strength in most experiments of either 150 or 300 mM formed by addition of sodium chloride. It was not possible to change the solution while maintaining trapping, so the different ionic strengths were tested in separate experiments.

Controlling flow-cell temperature

In experiments in which the temperature of the flow cell was varied, the temperature control was achieved by applying a thermal gradient across the glass surfaces driven from a pair of 40-W Peltier units in thermal contact with the objective. To reduce heat loss, there was an air gap between the condenser and the flow cell. The flow cell itself consisted of two coverslips supported by a Perspex spacer on the microscope stage.

A feedback system was employed between a thermocouple embedded in the aluminium cuff encasing the objective and the Peltier units. The calibration of temperature was performed by heating waxes of calibrated melting point inside the chamber. The flow-cell temperature could be varied between 10°C and 60°C and settled to ±1°C of the equilibrium temperature within 1 min of a change in command temperature. The presence of the laser-trap was found to increase the temperature in the vicinity of the focal waist by ~2°C, consistent with previous findings (Kuo, 1998).

There was no significant change in magnification with temperature, but there was a change in the height of the bead above the coverslip. This was manifest in an alteration in the focus of the bead image at the level of the detectors resulting in a different sensitivity. It was rectified by refocusing through *z* movement of the objective and recalibrating the detectors by oscillating the beads (tethered together) with a piezoelectric transducer-controlled mirror.

RESULTS

Force-extension experiment protocol and data fitting

In all the experiments on native titin, the molecule was attached to two beads, each labeled with an antibody to a different epitope. The procedure used (described in detail in the Materials and Methods section) was to introduce the two sets of beads into a flow cell, one of the sets of beads carrying a fluorescent marker. One bead from each set was trapped, and the two beads held apart. One of these beads was then moved using a triangular wave of 1–2 Hz so as to tap the second bead at one extreme of its motion. When an attachment (tether) had formed, the bead and trap positions were recorded while the triangular wave movement was continued or an alternative mechanical perturbation applied. The procedure used in the PEVK construct experiments was similar, except that the construct was chemically cross-linked to the beads (see Materials and Methods).

Fitting the data with all models described (Supplementary Materials) produced some results common to all data sets:

1. Worm-like chain fits of a given order n were always better than freely jointed chain fits of the same order (consequently only the worm-like chain results are given).
2. The addition of a small enthalpic component (elastic modulus K in the range 600–900 pN) improved some of the fits ($P = 0.1$–0.2) but never at the prescribed level of confidence of $P < 0.01$ (we therefore modeled the elasticity for all regions of titin as having a pure entropic basis, at least in the first place).
3. Higher order corrections to the pure entropic worm-like chain model made some improvement to most of the fits (again in the range $P = 0.1$–0.2) but not at the prescribed level of confidence of $P < 0.01$.
4. The highest order n of worm-like chains in series within any data set that improved the fit at a confidence level $P < 0.01$ was 2 and was only found for titin segments that included both the PEVK region and the tandem-Ig domains.
5. With further components added to a pure single worm-like chain model, there was found to be some evidence for systematic deviation for the whole skeletal muscle titin data sets possibly due to fitting of intrinsic noise as opposed to underlying signal (Supplementary Material). Also, there was some evidence for systematic deviations in the fitted parameters of multiorder worm-like chain models for data sets in which a single chain fit was adequate, which were consistent with applying the same fitting algorithms to theoretically generated noisy single worm-like chain force-extension data.

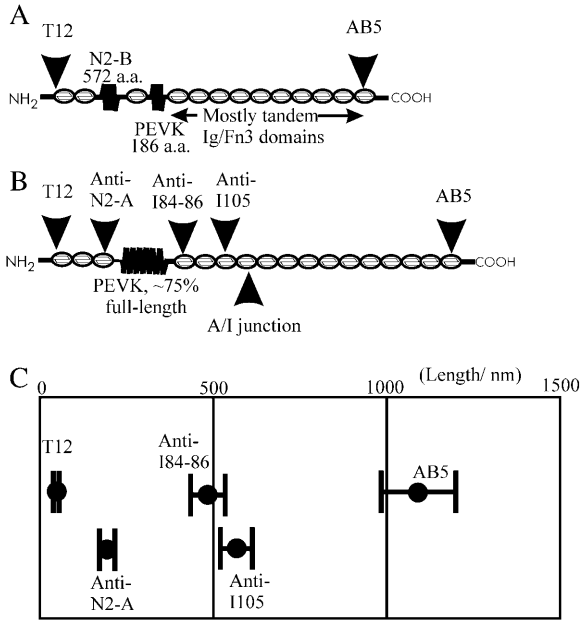

FIGURE 1 Schematic diagram of the two native titin isoforms used of (*A*) bovine cardiac, consisting predominantly of the N2-B isoform, and (*B*) rabbit longissimus dorsi. The epitopes for the antibodies used in this study have been marked with arrows. The number of residues in the PEVK region of the longissimus dorsi region has not been determined to date, though it is known to be less than that of the full-length isoform as expressed in soleus muscle (2181 aa). The results (*C*) from immunofluorescence labeling of rabbit longissimus dorsi muscle myofibrils (full results are given in Table 2) are superimposed on a ruler to be compared with *B*. Error bars are set at one standard deviation from the mean (●).

Position of antibodies

The loci of the known epitopes of the antibodies used are shown diagrammatically in Fig. 1. As these antibodies were not raised against the source of titin used in our experiments, rabbit longissimus dorsi, we checked the positions of binding sites in the sarcomere in myofibrils from this muscle using immunofluorescence (Materials and Methods). The results are shown in Table 2 together with the positions expected from sequence information. There is reasonable agreement between the two.

Force-extension relation of skeletal muscle native titin

Using the procedure for native titin described above, when a tether had been formed the triangular wave movement was continued, and the bead and trap positions were recorded. Force-extension curves were subsequently derived by averaging 20–30 cycles in the case of long-lived tethers and 5–10 cycles in the case of short-lived tethers. The maximal force was limited to <80 pN (Materials and Methods), and few incidences of rapid baseline shifts, corresponding to domain unfolding, were observed (the rate of stretch was in fact chosen to avoid unfolding Ig/Fn domains but slow enough not to require correction for viscous forces). Further, in the case of native titin, the force-extension relations derived from the two halves of the triangular wave cycle were in general identical, i.e., there was none of the hysteresis that accompanies unfolding (Tskhovrebova et al., 1997; Kellermayer et al., 1997; Rief et al., 1997), with only 10–20% of long-lived tethers exhibiting a very transient hysteresis that was not present beyond ~10 stretch cycles and beyond (Supplementary Material), similar to that observed from a previous study (Kellermayer et al., 2001). The rates of stretch used by Kellermayer et al. (2001) were in the range 40–100 nm s^{-1}, smaller by a factor of at least 30 than our rates of stretch, with a concomitant reduction in range of onset of unfolding to ~25–30 pN. The lack of steady-state hysteresis was found to be consistent with Monte Carlo simulations (Supplementary Material), which suggested that, for the relatively high ramp rates used here, Ig/Fn unfolding would occur mostly in the range 100–150 pN. In the case of the native PEVK region and the PEVK construct, hysteresis was normally present at the beginning of a run, and in the case of the construct hysteresis often persisted to a lesser extent throughout the

run. Evidence for stepwise lengthening accompanying the initial phase of hysteresis is dealt with in a later section.

Experiments on the skeletal (rabbit longissimus dorsi) muscle isoform employed antibody pairs chosen to select the following regions: the whole of the titin molecule from the Z-disk to M-line regions (for both the skeletal and cardiac isoforms), the A-band region, the I-band region, a tandem Ig domain region from the I-band, and the PEVK region. For each region, separate experiments were performed at ionic strength 150 mM and 300 mM. The results for the whole skeletal muscle titin molecule are given in some detail to illustrate the methods used, and the results for the other regions and for cardiac titin are presented more briefly.

Whole titin

The antibody pair used (T12-AB5) selects the whole of the molecule except for a region ~60 nm from the Z-disk. All force-extension curves were fitted with multicomponent freely jointed and worm-like chain models, both with and without enthalpic contribution (Supplementary Material). As shown in Fig. 2, the fits were qualititatively similar whichever model was used, though in both cases two components produced a better fit to the data than one component with a WLC model giving better fits than that of a freely jointed chain. This was the case for both of the two regions (whole molecule and I-band) of the molecule for which two chains in series were needed to fit the data, but for regions of the molecule for which a single chain sufficed (PEVK region, tandem-Ig region, and A-band), the data were better fitted by the WLC model, and for this reason (and for the sake of brevity) only the WLC-based analysis is presented here.

For the two-component fits for the whole molecule data set, though the quality of fit was variable, there was a tendency as seen in the example shown in Fig. 2 toward a poor fit in the low force region (<10 pN) where the fitted curves lay at slightly higher forces (maximal deviation ~ 1.5 pN) than the experimental data, whereas in the high force region (>50 pN) the fitted curves lay slightly below the experimental data. It is therefore not possible to entirely exclude other factors than two purely entropic elastic components.

The time-averaged force-extension curves derived for 56 bead pairs are shown in Fig. 3. Because no data were excluded, Fig. 3 includes both short-lived (5–10 s) and long-lived (5–20 min) tethers. The fits by one- and two-component worm-like chain models are compiled in Fig. 4, by plotting $1/L_p$ versus L_c. It is noticeable in both figures that the curves for long-lived tethers lie to one extreme of the length distribution, corresponding to long contour lengths. Supposing that the preincubated titin is specifically bound to the antibody on the bead via the epitope at the M-line, short-lived tethers are bound to the other bead nonspecifically, apparently at random along the length of the molecule.

There is little suggestion of a multimodal distribution in Fig. 3 as would be expected for multiple tethers. Further, when a tether broke, it did so in an all-or-none fashion. Also, the mean values of L_p for single chain fits for the long-lived tethers were in agreement with those of the short-lived tethers to within ~10%, implying that the same number of tethers were present. Coupled with an argument based on Poisson statistics concerning the likely frequency of multiple tethers (Supplementary Material), these observations suggest that the long-lived tethers are likely to be singular and specific. Further analysis of the fits appears at the end of this section.

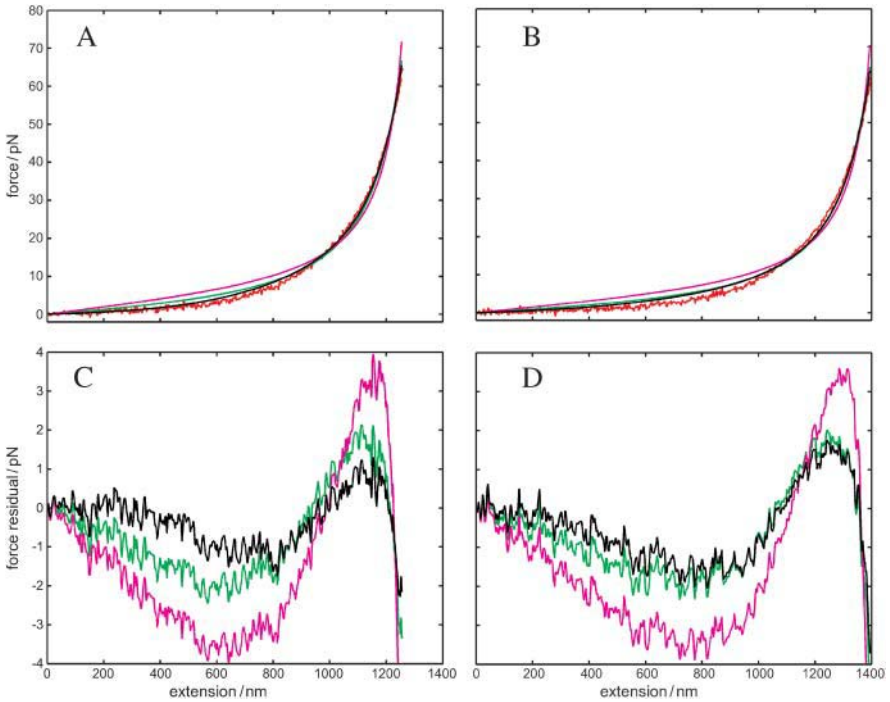

FIGURE 2 Force-extension relation for the whole titin molecule and polymer model fits. Force-extension curves at (*A*) 150 and (*B*) 300 mM ionic strength (*red*) with polymer fits of single freely jointed chain (*green*), single worm-like chain (*magenta*), and double worm-like chain (*black*). (*C*) Force residuals for the fits of *A*. (*D*) Force residuals for the fits of *B*.

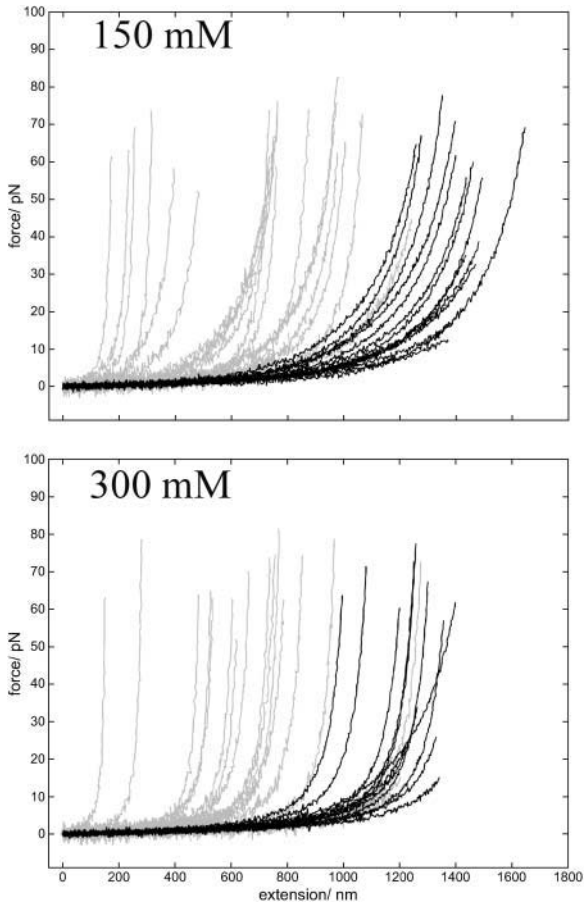

FIGURE 3 Complete data sets for time-averaged force-extension relations for the whole molecule at 150 and 300 mM ionic strength. Short-lived tethers (*shaded*) lasted less than 10 s before detachment. Long-lived tethers (*solid*) lasted at least 5 min of continuous stretch-release cycles before the experiment was terminated.

As regards the values of L_p and L_c for long-lived tethers, the values for the two components found in this study are similar but not identical in magnitude to those reported by Tskhovrebova et al. (1997). The short persistence length component (chain I) was identified by Tskhovrebova et al. with the PEVK region, and the experimental and theoretical values of L_c are in reasonable agreement (Tables 3 and 4). The value of L_p of 0.50 nm is roughly equivalent to an L_k of 1.0 nm, or to a chain segment length of $1.0/0.38 = 2.6$ amino acid residues, consistent with a polypeptide chain with some degree of hindered rotation. The long persistence length component (chain II) with a value of L_c of 966 nm is to be identified with the chain of Ig/Fn domains for the whole molecule, with a value of L_p of 3 nm and a segment length of ~6 nm, corresponding to flexibility over a stretch of ~1–2 neighboring domains.

The tendency toward a poor fit between the calculated and experimental force-extension curves noted above was investigated further. Constraining the values of L_p and L_c for chain I to the average for the data set resulted in slightly improved fits in the low force region and gave higher values of L_p (range 3–8 nm) for chain II, though with a much increased scatter in L_c. Thus the value of L_p for chain II may be an underestimate.

Chain I was sensitive to ionic strength, with the value of L_p changing from 0.50 nm at 150 mM to 1.7 nm at 300 mM (Table 4), whereas chain II was not affected by ionic strength.

A-band region

The antibody pair used was anti-I105-AB5. This demarks a region consisted of the entire A-band component plus a small 13 Ig/Fn domain segment of the I-band (Table 2 and Fig. 1). The results of single WLC modeling are shown in Fig. 5, upper left panel. At first sight it is surprising that the curves for short-lived tethers lie to the low L_c side of the curves for long-lived tethers: titin was precomplexed with the M-line antibody (AB5), and thus there is no apparent reason why short-lived (nonspecific) tethers should not have spanned the entire length of the molecule. However, there are few full-length short-lived tethers in any of the experiments, implying that the Z-line end of the molecule is either not as accessible as the rest of the molecule or that it was often truncated (Nave et al., 1989).

It was found that there was no statistically significant improvement to the fits in going from a single to a double chain model, based on Student's *t*-tests between the root mean-square (rms) value of the residuals for each fit at a confidence level of $P < 0.01$ (Supplementary Material). The single component has the same value of L_p as chain II of the whole molecule, and correspondingly there was no effect of increased ionic strength. The value of L_c was 1039 nm and was not significantly different at higher ionic strength. It follows that chain I found for the whole molecule does not lie in the A-band region (Table 5).

Tandem Ig (I-band)

The tandem Ig region selected in the I-band region consists of ~20 IgI between the anti-I84–86 and I41 loci (Fig. 1 and Table 2). The force-extension curves were fitted adequately with one chain (Table 5 and Fig. 5), whose persistence length was consistent with chain II of the whole molecule and that was unaffected by changes in ionic strength. This serves as a control and shows that chain I is unlikely to derive from the I-band Ig domains, supposing that the anti-I84–86-I41 region is typical of the whole of the I-band.

I-band region

The I-band region was selected by using the T12 and anti-I105 antibodies, the anti-I105 antibody mapping 50–60 nm on the N-terminal side of the A/I junction (Fig. 1 and Table 2). The I-band region force-extension data were best fitted by a two-component model, with values of L_p similar to those found for the two components of the whole molecule, and

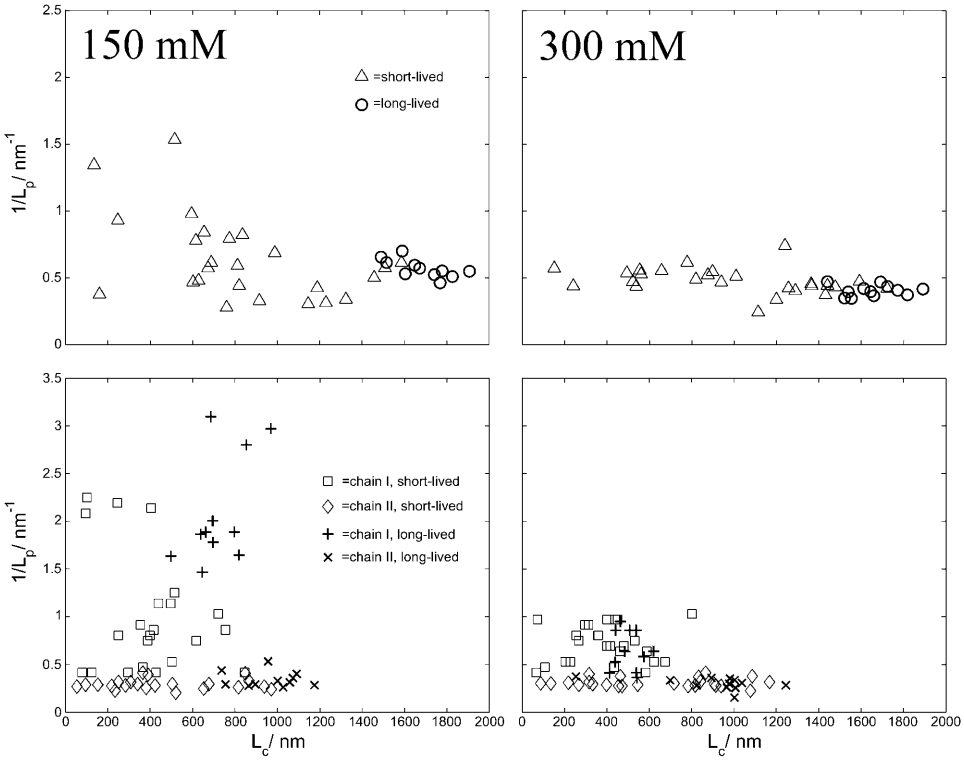

FIGURE 4 Plots of $1/L_p$ versus L_c for the whole molecule at 150 and 300 mM ionic strength. (*Upper row*) Single worm-like chain fits, short-lived tethers (△), and long-lived tethers (○). (*Lower row*) Double worm-like chain fits, short-lived tethers (□ and ◇ for chain I and II, respectively), and long-lived tethers (+ and × for chain I and II, respectively).

with values of L_c of 507 and 374 nm for chains I and II, respectively (Table 5 and Fig. 5). Only the short persistence length component was sensitive to ionic strength. It follows that chain I lies within the I-band region. Most curves exhibited little obvious signs of hysteresis, similar to the whole skeletal muscle titin stretch data, with only one tether in the 150-mM data set and two in the 300-mM data set showing some small transient hysteresis that lasted less than 10 consecutive stretch-release cycles.

TABLE 3 Polymer parameters for whole titin molecule from other studies

		L_{k1}/nm	L_{c1}/nm	L_{k2}/nm	L_{c2}/nm
Sequencing*†‡‡††	Cardiac	0.34–0.38	67		1100
	Skeletal	0.34–0.38	530–840		1230–1350
NMR§¶				4.4–4.6	
Molecular-combing‖**	Skeletal		150–500	4–6	1000–1200
In situ epitope†**	Skeletal		500–700		1200–1300

*Labeit and Kolmerer (1995).
†Linke et al. (1996).
‡Freiburg et al. (2000).
§Pfuhl and Pastore (1995).
¶Goll et al. (1998).
‖Tskhovrebova and Trinick (1997).
**This article.
††In using the sequence data, the values of L_{c1} refer to the anticipated length of the PEVK region assuming that it is fully denatured, i.e., has a Kühn length equal to that of the mean peptide α-carbon spacing; values of L_{c2} have been computed on the basis that it consists of folded Ig domains, the number of which is indicated from the sequence data, with an average length 4.4 nm.

PEVK region

Antibodies anti-N2-A and anti-I84–86 were used to select the PEVK region (Fig. 1 and Table 2). The steady-state force-extension curves of long-lived tethers were fitted adequately by a single worm-like chain model (Table 6). The persistence length (0.91 nm) and contour length (533 nm) show that this corresponds to chain I of the whole molecule, and as expected L_p is sensitive to ionic strength. Thus chain I corresponds to the PEVK region. More detailed results on the dependence of the polymer parameters on ionic strength and on temperature are given below.

PEVK construct

The construct begins 24 residues on the N-terminal side of the PEVK region, with the remaining 526 residues being ~25% of the full-length skeletal muscle PEVK region with no deletions or insertions. After the first ~10 cycles in which stepwise lengthening and shortening was apparent (cycles that were excluded from this quasi-steady-state analysis), there was usually some residual hysteresis between stretch and release cycles, and fits were applied only to the time average of the release half-cycles at forces greater than 5 pN, on the grounds that stress relaxation was generally only

TABLE 4 WLC fits to force-extension data for whole skeletal muscle titin

Results of one-WLC fits for whole titin							
		L_p/nm		L_c/nm			
Skeletal		Mean	SE	Mean	SE	σ_{fit}/pN	n
Whole	150 mM	1.8	0.1	1686	40	0.24	11
	300 mM	2.5	0.1	1655	38	0.24	12

Results of two-WLC fits for whole titin											
		L_{p1}/nm		L_{c1}/nm		L_{p2}/nm		L_{c2}/nm			
Skeletal		Mean	SE	Mean	SE	Mean	SE	Mean	SE	σ_{fit}/pN	n
Whole	150 mM	0.50	0.10	723	39	3.0	0.2	966	42	0.17	11
	300 mM	1.7	0.2	505	81	3.6	0.3	909	70	0.18	11

The antibody pair used was T12-AB5. σ_{fit} is the standard deviation in force between the theoretical values and the data. n is the number of long-lived tethers generated (from different bead pairs) in each data set.

observed on the stretch half-cycles, with very little apparent recovery observed at forces greater than around the 5-pN level. The force-extension curves of long-lived tethers were fitted adequately by a single worm-like chain model (Table 6 and Fig. 6). The value of L_p of 1.80 nm is twice as high as the value found for native PEVK, but it depended in a similar fashion on ionic strength, more than doubling in value between 150 and 300 mM (Table 6), the value of L_c being 201 nm at 150 mM and not significantly different at 300 mM.

Force-extension relation of cardiac muscle titin

The same antibodies (T12 and AB5 epitopes) were used as for the whole skeletal muscle molecule. The data were fitted adequately by a single component worm-like chain model (Table 7 and Fig. 6). Unlike the results from stretches on the skeletal muscle isoform it was found that there was relatively little improvement in fit in going from a one to a two-component model, nor from a one to a three-component model (Watanabe et al., 2002; Li et al., 2002). The value of L_p corresponds to Ig/Fn domains and is not sensitive to ionic strength. As the PEVK region is 167 residues long in the cardiac muscle isoform, these results reinforce the conclusion that the small persistence length chain I of skeletal muscle titin derives from the PEVK domain. The result is consistent with simulations that suggest the elastic contributions from by the PEVK and N2-B regions to the total elasticity of whole cardiac muscle titin are very small over the low force range used here (Supplementary Material).

Summary of skeletal and cardiac muscle titin force-extension results

Table 7 collates the results of polymer modeling using the best fits from either one or, where appropriate, two worm-like chains. As already noted, the long persistence length chain II, observed for all the regions except the PEVK region, is consistent with a flexible chain composed of Ig or Ig/Fn domains, with an average value over all the data of L_p of 2.9 nm at 150 mM and 3.1 nm at 300 mM. Only the contour length varies substantially with the different antibody pairs used. The short persistence length, ionic strength-dependent chain I found in skeletal muscle whole titin, I-band, and PEVK regions is consistent with an unfolded peptide chain in the PEVK region (though evidence for a partially folded substructure is given below). The average value over all the data of L_p is 0.76 nm at 150 mM and 1.33 nm at 300 mM.

The contour lengths obtained from the fits are plotted against the extended lengths predicted from sequence information of the soleus muscle titin isoform in Fig. 7. There is reasonable agreement between most of the experimental values of L_c and the predicted values, though there is some deviation especially for the highest contour lengths, consistent with the presence of fewer Ig domains and a shorter PEVK region in longissimus dorsi compared to the soleus sequence. The simplest interpretation of these results is that over the range of forces examined, the elastic properties of skeletal muscle titin can be described by two chains in series, one (chain I) deriving from the PEVK region and the other (chain II) from the chain of Ig/Fn domains. Only the PEVK region is affected by ionic strength.

The fact that the elasticity of whole cardiac muscle titin is adequately described by a single worm-like chain appears to contradict previous single molecule studies of the N2-B region flanked by only a few Ig domains. These studies suggested the presence of three independent components due to the tandem-Ig domains, the PEVK, and the N2-B regions (Watanabe et al. 2002; Li et al., 2002). However, simulations show that, for stretches on the whole cardiac muscle titin molecule, the PEVK and N2-B components will have much smaller fractional extensions than the tandem-Ig region by a factor as high as 10 over the range of force used here, equating to extensions as low as ~20 nm for the N2-B region, and so the elasticity is dominated by the tandem-Ig

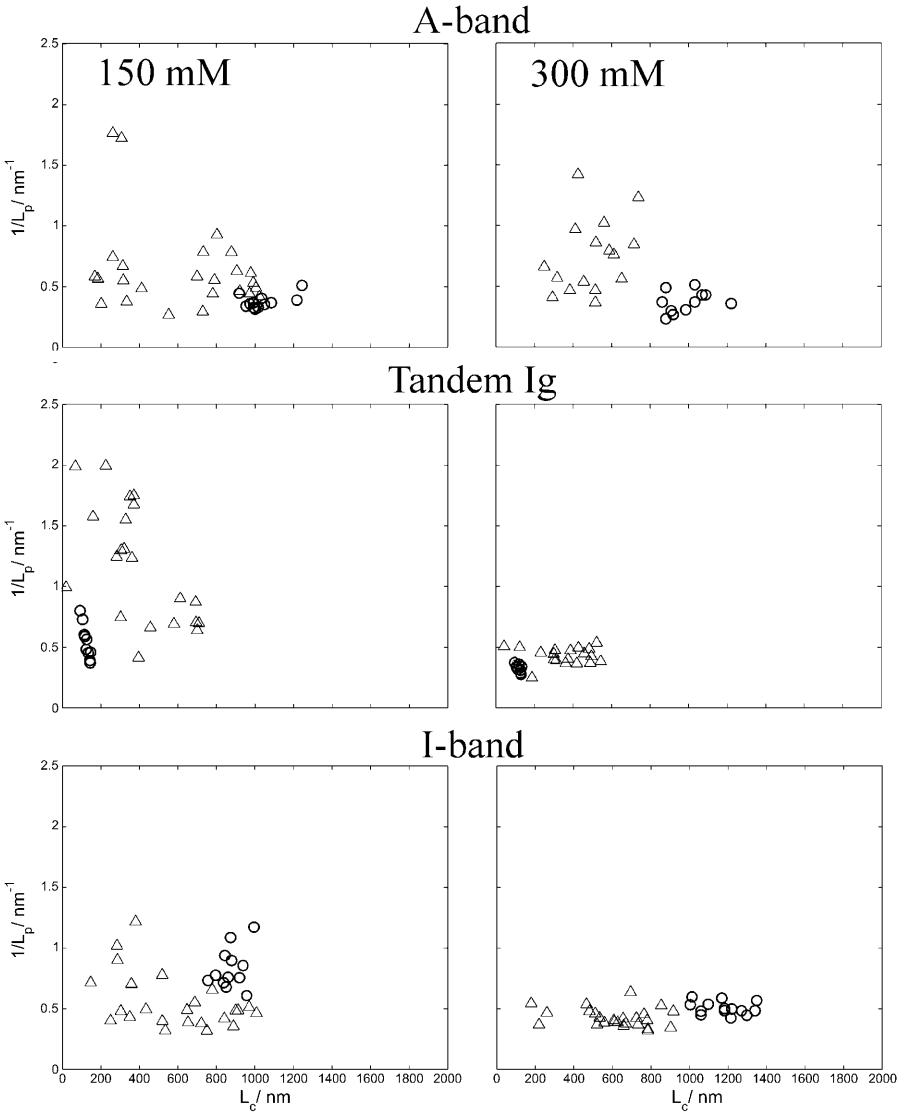

FIGURE 5 Plots of $1/L_p$ versus L_c for double WLC fits for A-band, tandem Ig's, and I-band at 150 mM and 300 mM ionic strength. Short-lived tethers (△) and long-lived tethers (○) for A-band region anti-I105-AB5 (*top row*), tandem Ig region anti-I84–86-anti-I105, (*middle row*), and I-band region T12-anti-I105 (*bottom row*).

region (Supplementary Material). Greater extensions at higher force would be needed to resolve the PEVK and N2-B components.

Force-extension relation of PEVK region: ionic strength, temperature, and pH dependence

As the PEVK region showed a marked dependence on ionic strength, we investigated the dependence in more detail, and we also measured the effect of change of temperature. We attempted to do these experiments on both the native PEVK region and the PEVK construct, but experiments on the former were limited to the effect of ionic strength, as the antibody binding became too weak with substantial increase of temperature. The effect of changing pH was also investigated, though problems associated with weakening of tether binding restricted the range to only 1–2-pH units, and no significant changes in elasticity over this range were detected.

Ionic strength

The force-extension relation was measured as a function of ionic strength over the range 15–300 mM. Fitting the force-extension curve of long-lived tethers with a WLC model resulted in the relation of L_p and L_c to ionic strength shown in Fig. 8 *A*. The upper pair of curves is for the PEVK construct and the lower pair for native PEVK. Both show little or no systematic change in L_c but a marked dependence of L_p on ionic strength. As the Debye-Hückel electrostatic screening effect depends on the inverse of the square root of ionic strength, the data are replotted on a log-log scale in Fig. 8 *B*. This reveals that the dependence on ionic strength is 1.4 and 1.8 power for native and construct PEVK, respectively, much higher than is expected from screening effects alone.

TABLE 5 WLC fits to force-extension data for discrete regions of skeletal muscle titin

(*a*) Results of one-WLC fits for the I- and A-band, and a region in the I-band consisting only of tandem Ig-like domains*

Skeletal		L_p/nm		L_c/nm		σ_{fit}/pN	n
		Mean	SE	Mean	SE		
A-band	150 mM	2.7	0.1	1039	29	0.24	12
	300 mM	2.5	0.1	1055	38	0.29	12
I-band	150 mM	1.2	0.1	875	20	0.27	12
	300 mM	2.0	0.1	1175	31	0.27	14
Tandem Ig	150 mM	3.3	0.2	125	6	0.25	7
	300 mM	3.4	0.2	118	5	0.24	10

(*b*) Results of two-WLC fit results for I-band region†

Skeletal		L_{p1}/nm		L_{c1}/nm		L_{p2}/nm		L_{c2}/nm		σ_{fit}/pN	n
		Mean	SE	Mean	SE	Mean	SE	Mean	SE		
I-band	150 mM	0.79	0.06	507	25	3.1	0.3	374	20	0.19	12
	300 mM	1.3	0.1	421	19	3.3	0.1	415	15	0.18	14

*The antibody pairs used were as follows: A-band, anti-I105-AB5; I-band, T12-anti-I105; and tandem Ig, anti-I84–86-anti-I105.
†The antibody pair used was T12-anti-I105.

The extrapolation of L_p to zero ionic strength gives a value of ~0.2 nm, close to the expected value of a fully flexible polypeptide chain. If the variation in persistence length with ionic strength has its origin in Debye-Hückel screening, the power dependence implies a complex effect, possibly involving hydrophobic effects (see Discussion).

Temperature

Though it was possible in principle to vary the temperature over the range 10–60°C while holding the same bead pair, in practice the tether usually broke as the temperature was raised before a full data set could be obtained, presumably because the rate of dissociation increases with temperature. However, for eight tethers data were collected over a reasonable range of temperatures. One set of force-extension curves for the same tether is shown in Fig. 8 *C*. It is clear that at a given extension force rises markedly as the temperature is raised. All eight sets of values of L_p and L_c (using single WLC fits of long-lived tethers) are plotted against temperature in Fig. 8 *D*. L_p shows a decrease as the temperature is raised, and (surprisingly) the value of L_c also decreases.

In an entropic model (worm-like chain or freely jointed chain), force at a fixed extension should be proportional to the absolute temperature, and thus it should vary by ~60/270 = 25% over the range studied, whereas the relation is clearly much steeper. It appears that the construct adopts a more compact form as the temperature is raised (lower L_p), with part of the molecule no longer compliant (lower L_c) over the range of forces applied.

Hysteresis in the PEVK region

Transient hysteresis in long-lived tethers was observed in the nonaveraged force-extension curves for the PEVK component, both in the native PEVK region and the PEVK construct, principally within the first 10 stretch-release cycles and then rarely for subsequent cycles. Hysteresis implies the presence of stress relaxation, and in many records there was direct evidence for stepwise stress relaxation, though the lack of significant hysteresis in the whole skeletal muscle titin and I-band data sets seems possibly to contradict this result as is discussed later (Discussion).

PEVK construct

Two successive stretch-release cycles from the start of an experiment are shown in the record of Fig. 9 *A* taken at an ionic strength of 15 mM for a long-lived tether. This particular record was selected as it showed the greatest number of lengthening steps. The force-extension plots (Fig. 9 *B*) show stepwise lengthening, visibly with 7–9 steps.

TABLE 6 WLC fits for force-extension data for the native PEVK region and PEVK construct

PEVK		L_p/nm		L_c/nm		σ_{fit}/pN	n
		Mean	SE	Mean	SE		
Native	150 mM	0.91	0.05	553	22	0.17	7
	300 mM	2.71	0.47	580	26	0.11	10
Construct	150 mM	1.80	0.35	201	9	0.20	8
	300 mM	4.33	0.93	198	10	0.33	9

The antibody pair used for the native PEVK region was anti-N2-A-anti-I84–86.

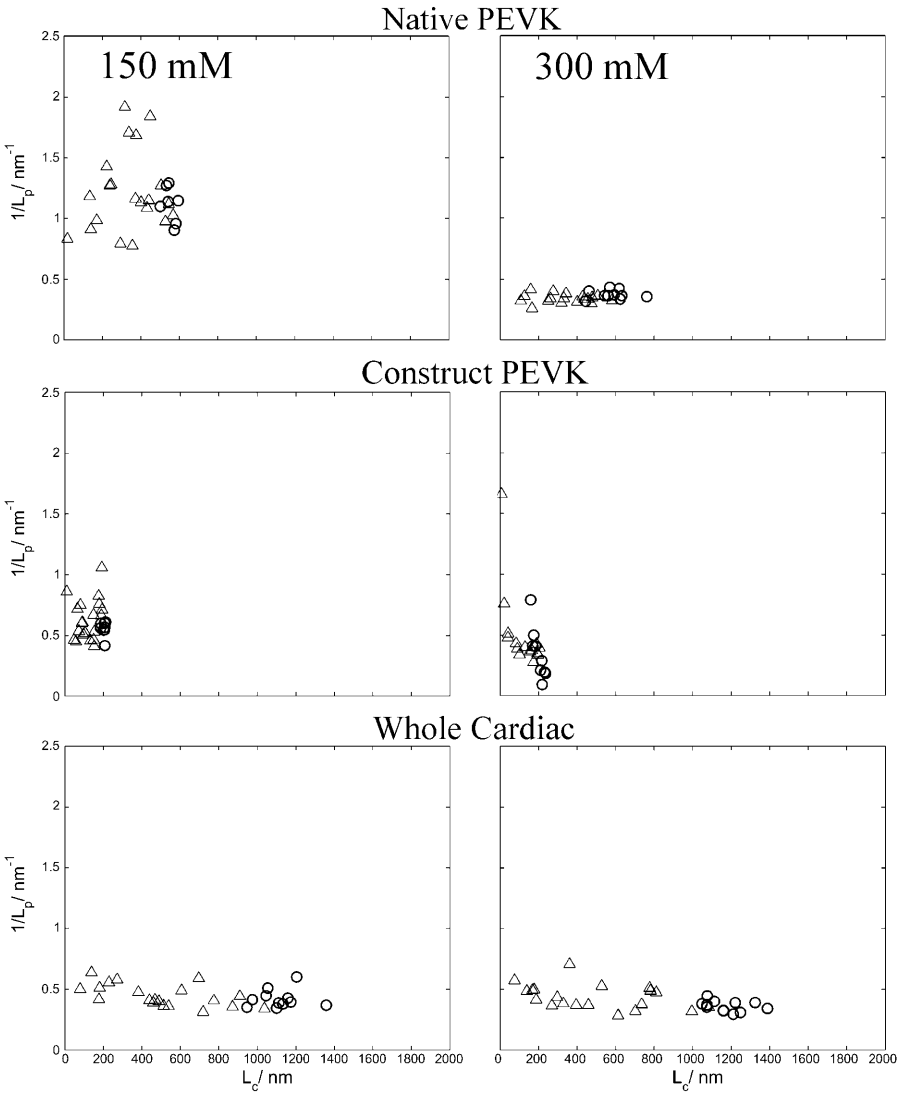

FIGURE 6 Plots of $1/L_p$ versus L_c for single WLC fits for the native PEVK region, the PEVK construct, and for the whole molecule of cardiac muscle titin at 150 and 300 mM ionic strength. Short-lived tethers (△) and long-lived tethers (○), for the native PEVK region N2-A to anti-I84-86 (*top row*), 550-aa PEVK construct (*middle row*), and whole bovine cardiac titin region T12-AB5 (*bottom row*).

Chung-Kennedy edge detection (Chung and Kennedy, 1991) was performed on the data using a threshold *t*-statistic of 8 (Supplementary Material), and the raw step lengths were measured for those steps found to be statistically significant. The distribution of step lengths lumps together steps that occurred at different levels of force, and because of the nonlinearity of force-extension relation, the step lengths need to be standardized. This can be achieved by fitting theoretical polymer curves to the force-extension relation of Fig. 9 in between steps (Rief et al., 1997) and then using differences between the resulting contour lengths (Supplementary Material). The results are shown overlaid on the force-extension data of Fig. 9 *B*, and a plot of $1/L_p$ versus L_c is shown in Fig. 9 *C*.

In Fig. 9 *B*, the initial value of L_c immediately after the beginning of the stretch was ~10 nm, and L_p was ~0.05 nm. As shown in Fig. 9 *C*, after the first two detected steps L_c is ~120 nm and L_p ~ 0.3 nm, and in the remaining five steps the changes in L_c for each step are 24, 12, 8, 25, and 14 nm, and L_p is approximately constant. The record in Fig. 9 showed the widest range of steps observed, but changes in L_c varied at the start of different experiments; in some cases the initial value of L_c before a detectable step was greater than 50 nm, and in the subsequent steps L_p was again constant. Therefore there seem to be two lengthening processes; an early one at low force, variable in occurrence and with a changing value of L_p, and a later process at a higher force and consisting of a series of step changes in L_c at a nearly constant L_p (though the errors are such that the difference in the values of L_p is only just statistically significant at a confidence level of $P < 0.1$). The values of L_p in both regions were found to show a similar dependence on ionic strength as noted earlier (Fig. 8 *A*), rising from 0.05 to 0.2 nm for the early phase and from 0.3 to 1.8 nm for the late phase, as ionic strength is increased (though again with a high associated error). The number of later steps varied from zero to seven. Ionic strength (15–300 mM) had no significant effect of the size of the basic step and did not affect the

TABLE 7 Summary of WLC fits for skeletal and cardiac muscle titin

Skeletal		L_{p1}/nm	L_{c1}/nm	L_{p2}/nm	L_{c2}/nm	n
Whole	150 mM	0.50 ± 0.10	723 ± 39	3.0 ± 0.2	966 ± 42	11
	300 mM	1.70 ± 0.20	505 ± 81	3.6 ± 0.3	909 ± 70	12
A-band	150 mM	–	–	2.7 ± 0.1	1039 ± 29	12
	300 mM	–	–	2.5 ± 0.1	1055 ± 39	12
I-band	150 mM	0.79 ± 0.06	507 ± 25	3.1 ± 0.3	374 ± 20	12
	300 mM	1.30 ± 0.10	421 ±19	3.3 ± 0.1	415 ± 15	14
Tandem Ig	150 mM	–	–	3.3 ± 0.2	125 ± 6	7
	300 mM	–	–	3.4 ± 0.2	118 ± 5	10
PEVK*	150 mM	0.91 ± 0.05	553 ± 22	–	–	7
	300 mM	2.71 ± 0.47	579 ± 26	–	–	10
PEVK1†	150 mM	1.80 ± 0.35	201 ± 9	–	–	8
	300 mM	4.33 ± 0.93	198 ± 10	–	–	9
			Cardiac			
Whole	150 mM	–	–	2.7 ± 0.1	1115 ± 34	11
	300 mM	–	–	2.8 ± 0.1	1175 ± 31	12

*Native PEVK region.
†PEVK construct.

probability for stepping. Temperature increase from 10 to 60°C similarly did not alter the basic step size significantly but did result in a slight increase in the mean number of steps observed for a stretch half-cycle.

The distribution of the amplitude of steps in contour length during both stretch and release half-cycles for long-lived tethers is shown in Fig. 10 *A*. Three positive extension peaks are resolved, which can be fitted by a series of Gaussian curves based on multiples of an ~10–12-nm basic step; if the whole set is fitted by an integral multiple of a basic step, its value is 11.1 nm. There are a few negative-going (i.e., increasing force) steps as well as the predominantly positive-going steps. The negative-going steps occurred at forces less than 20 pN; although too few in number to justify Gaussian fitting, there appear to be peaks at ~−10 and ~−20 nm. Autocorrelation analysis (Supplementary Material) on this histogram and that for square wave stretches (Fig. 10 *D*) suggested a periodicity of ~12.3 nm, which agreed reasonably well with the observed peak spacing. The modal value occurs at ~24 nm, double the basic step. This could arise from a number of reasons: 1), the Chung-Kennedy detector might miss many of the single steps; 2), the real basic step might be 24 nm, but there were a number of instances of double tethers, where the effect of a step in one molecule is halved; and 3), there might be cooperativity between the units (modules) underlying the steps, for example the lengthening of one module might destabilize a neighboring module. Experiments using square wave stretches (next section) suggest that the first explanation is the correct one.

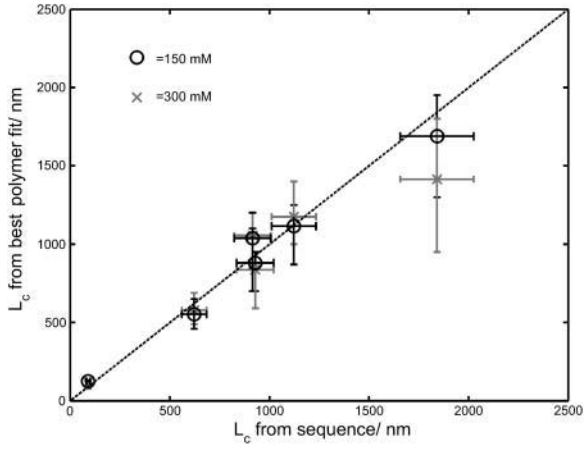

FIGURE 7 Comparison of total contour length from WLC fits with contour length predicted from the soleus muscle titin isoform sequence. (*Vertical bars*) Total range of fitted contour lengths. (*Horizontal bars*) Error of 10% of the predicted contour length from the sequence. (*Solid line*) Theoretical 1:1 plot. Ranges of contour length rather than errors are plotted as the preparation used may have contained a number of isoforms of different length; the error in contour length is included as a guide to the distribution of length.

With each lengthening event, as well as an increase in the contour length, there was in general a small increase in the persistence length, even in the late phase of lengthening. This can be explained by the preexistence of a structure (from earlier lengthening processes) with a low value of L_p; when the later lengthening events occur and lengths of chain with a higher value of L_p are thrown into series, fitting the combined structure with a single L_p will result in a successive increase in L_p.

The lengthening process might be explained by the breaking of multiple tethers, since L_p increases, but since L_c clearly also changes this seems unlikely (additional counterarguments are given in the Discussion). This is because the apparent persistence length of n parallel tethers is equal to L_p/n, and as each tether breaks, there is an increase in apparent persistence length by $L_p(1/(n-1) - 1/n)$ but no change in L_c. Whether the later lengthening process is due to unfolding of structural modules or to stepwise desorption of the molecule from the surface is dealt with in the Discussion.

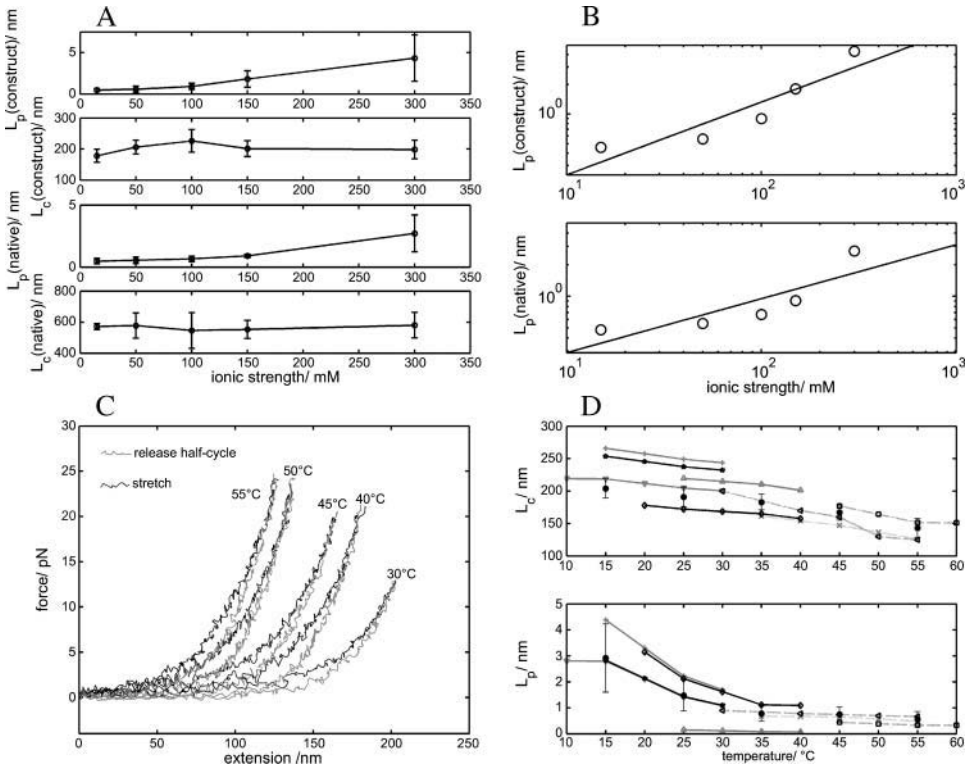

FIGURE 8 (*A*) Dependence of persistence length (L_p) and contour length (L_c) on ionic strength for PEVK construct (*upper pair* of *plots*) and native PEVK region (*lower pair* of *plots*) for long-lived tethers. Error bars are one SE of the mean. (*B*) Double logarithmic plots of L_p against ionic strength, with regression lines; (*upper*) PEVK construct; (*lower*) native PEVK region. Effect of temperature on force-extension relation of PEVK construct (for long-lived tethers): (*C*) Variation in force-extension relation with temperature for the same tether and (*D*) dependence of contour length (*top*) and persistence length (*bottom*) on temperature from single WLC fits. Data points connected by a line represent a single tether. ● are the mean values of the parameters after binning of all data over a 10°C range; error bars are one standard deviation from this mean.

Stepwise stress relaxation was observed more clearly when square wave stretches were applied (Fig. 10, *B* and *C*). Tethers were generated using the same tapping protocol and, as with triangle wave stretches, bead 1 held in positional feedback whereas the other bead was moved by applying a square wave of frequency 1–2 Hz to the galvanometer mirrors of trap 2 such that the force on the PEVK tether would be zero for half a cycle and nonzero for the other half, the value of which was determined by the chosen amplitude of the square wave.

There was a single peak in the raw extension step at 7–8 nm, but no values for negative extension-steps; however, the minimal force applied in these experiments was 25 pN, larger than the maximal force at which negative-going steps were seen in triangle wave experiments. As in the triangle wave experiments, it was necessary to standardize steps by correcting for the differing force at which they occurred, by estimating the change in contour length at each step. This was less straightforward than for triangle wave experiments since there is no interstep stretch of the force-extension relation to fit. However, WLC fits to the triangle wave stretch data can be compiled into a look-up table for contour and persistence lengths corresponding to points on the force-extension plane, allowing the equivalent contour and persistence lengths for square wave stretch data to be predicted after appropriate extrapolation. The result is shown in Fig. 10 *D*.

Unlike the result from triangle wave stretches, the modal value of step size is the same as the basic step size of ~12 nm. A possible explanation is that in all cases the two adjacent Chung-Kennedy detection windows run parallel to the time vector and not parallel to the vector of mean slope of extension with respect to time, unless a square wave stretch is employed. For triangle wave stretches, the molecule stiffens with increasing time and so the difference in mean extension values between adjacent detection windows either side of a true step event is lower than is the case for square wave stretches, hence lowering the likelihood for detecting small events. Thus more of the basic step events are missed for triangle wave stretches compared to square wave stretches.

Native PEVK

Stress relaxation was also observed for stretches on long-lived tethers of the native longissimus dorsi muscle titin PEVK region, using the antibody bead-conjugation technique to select the region bounded by the anti-N2-A and anti-I84–86 epitopes. The hysteresis between stretch and release half-cycles, which occurred only for the first ~10 cycles, was more dramatic than for the PEVK construct (Fig. 11 *A*). However, the Chung-Kennedy detector performed badly in general. With a few individual stretch cycles it was possible to detect step-like events (Fig. 11 *B*), both positive-going and negative-going, with the change in contour length being in the range 10–40 nm. However, in general the slope of the extension signal changed more rapidly than could be resolved by the 20-ms detection window, consistent with multiple stepping within the window, though lowering the window size resulted in an unacceptable number of false-positive

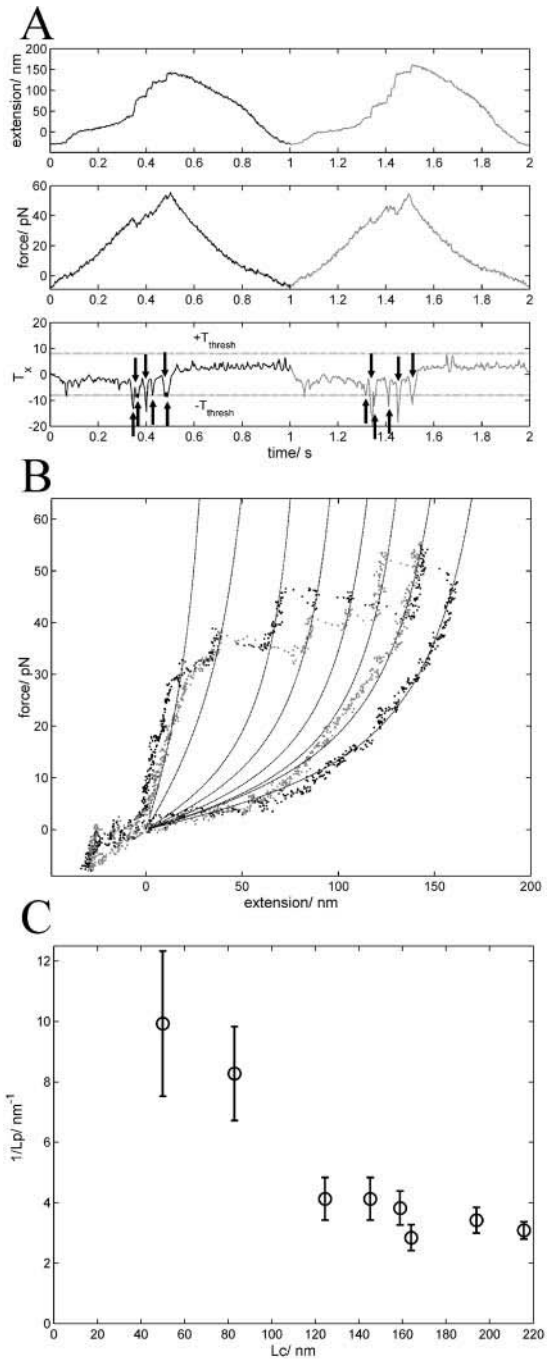

FIGURE 9 Stepwise lengthening from triangle wave stretches of the PEVK construct for long-lived tethers. (*A*) Force and extension records and the Chung-Kennedy *t*-statistic output. For clarity, only two consecutive stretch-release cycles are shown (*solid* and *shaded*, respectively). Arrows mark the position of detected steps. (*B*) The equivalent force-extension relation for each cycle in *A*. Single WLC fits are overlaid on each interstep region of the force-extension relation. (*C*) Plot of $1/L_p$ versus $1/L_c$ for the fits in *B*. Ionic strength was 15 mM.

detection events, and no reliable statistics could be obtained to confirm the size of a basic step. Overlaying many force-extension relations from consecutive stretch-release cycles (Fig. 11 *C*) gives a total range of contour length between 50 and 400 nm, consistent with ~30 stress-relaxation events of a 12-nm basic step.

DISCUSSION

Multiple tethers

It was important in this study to establish whether or not the formation of multiple tethers was a frequent occurrence, as the assumption of a single tether when multiple tethers are present gives erroneous results for polymer fits to force-extension data. A number of lines of evidence suggest that multiple tether formation was rare in our experiments:

i. The number of titin molecules in range of binding was small. ELISA measurements of native titin bound to antibody-coated beads showed that there were ~20 titin molecules bound per bead (Materials and Methods). The geometry of the bead-bead interaction shows that when the two beads (one complexed with the titin and the other not) were closer than the mean end-to-end distance of the molecule, ~90 nm in the instance of whole titin (Tskhovrebova and Trinick, 2001), only ~2.5% of the surface area of a 2-μm diameter bead and therefore ~0.5 titins were within the range of antibodies of the uncomplexed bead (our unpublished calculation). For the PEVK construct, less than 0.5% of the surface of a bead was likely to be within the range of a free maleimide site on the uncomplexed bead and correspondingly fewer molecules within range.

ii. Transient, nonspecific attachments had similar elastic properties to the long-lived specific tethers and thus derive from the same number of tethers formed; it is unlikely that this could happen consistently unless on each occasion only one tether was formed.

iii. It was rare for a further stable increase in stiffness to be observed after the formation of a tether. This may be because the presence of the tether restricted the relative motion of the beads, but it implies there was rarely a second available molecule within range of the first tether(s).

iv. The rate of tether formation was low, approximately one tether formed for 1000 contacts. Poisson statistics show that in this case the probability of multiple (greater than one) tether formation is ~1 in 10^4 (Supplementary Material).

v. Abrupt finite changes of L_p, corresponding to one of several tethers breaking, were rarely seen; when a long-lived tether broke, tension usually fell to zero.

vi. The distribution of values of L_p in each set of experiments was narrow, the standard deviation being 0.1–0.25 of the mean. Thus there was no evidence for integer multiple values of $1/L_p$ for either native titin or the PEVK construct for long-lived tethers. For short-lived tethers of whole titin, it was not possible to

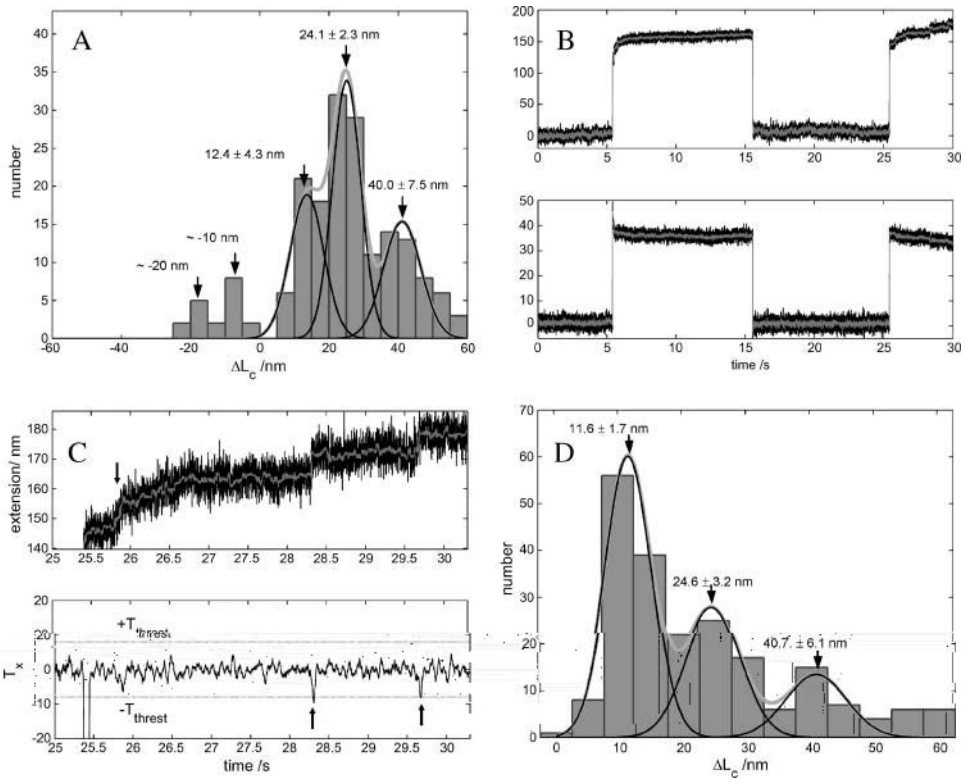

FIGURE 10 (*A*) Distribution of lengthening step size for triangle wave stretches of PEVK construct for long-lived tethers from eight bead pairs after Chung-Kennedy edge detection (20-ms window size and a *t*-statistic detection threshold of 8), using 5-nm bins. A total of 193 steps were detected, 27 negative extension steps and 166 positive extension steps. Fits for a three-Gaussian unconstrained fit for positive steps are shown (*shaded*) with the individual Gaussians (*solid*); Gaussian widths shown above each peak. Imposing the constraint that each peak should be an integer multiple of a unitary value produced a slightly worse fit with a unitary peak of 11.1 nm. Statistical tests confirmed that the Gaussian peaks were real and distinct at a confidence level $P < 0.01$. Square wave stretches on the PEVK construct for long-lived tethers: (*B*) force and extension records and (*C*, *top*) expansion of data from *B*, and (*bottom*) *t*-statistic output of Chung-Kennedy edge detection routine, window size of 20 ms with *t*-statistic threshold for step acceptance set at 8. (*Arrows*) Position of detected steps. (*D*) Distribution of the lengthening step size for square wave stretches on PEVK construct for long-lived tethers (26 bead pairs, window size of 20 ms, and *t*-statistic threshold of 8; bin size is 5 nm) distribution of contour length step size binned in 5-nm intervals. Unconstrained three-Gaussian fit (*shaded*) and the individual Gaussians (*solid*). Constraining the peaks to be integer multiples of a unitary value led to a slightly worse fit with a unitary peak of 10.5 nm. Vertical errors on the histograms bars are ~3%.

differentiate on the basis of L_p values alone whether random binding had occurred across different segments of a titin monomer (thus including the PEVK region in the stretched segment or not) or if random binding had occurred across the length of a titin dimer, since the spread in L_p was significantly greater than for the long-lived tether data sets (Supplementary Material).

Some of the arguments above would be affected if the titin were to be oligomeric (Tskhovrebova and Trinick, 1997) or aggregated (Tskhovrebova and Trinick, 2002), though we were careful in the case of skeletal muscle titin to take a sample fraction that was monomeric, and EM micrographs of straightened titin molecules showed no signs of self-association. However, it is possible that the titin reaggregated with storage, and the cardiac muscle titin certainly was oligomeric. A further complication is that the antibodies used were bivalent. On balance, though, the weight of evidence suggests that long-lived tethers were monomers.

Values of L_p and L_c

The results show clearly that the elasticity of the skeletal muscle isoform cannot be represented adequately by a single entropic spring but is consistent with two entropic springs acting independently in series, as first shown by Tskhovrebova et al. (1997). Here, in addition, using the same antibody-delimitation approach, we have performed stretches on the I- and A-band regions of the molecule, together with the PEVK region and a tandem Ig zone of the I-band, and found evidence (summarized in the Results section) that the short-persistence length component (chain I) is indeed located in the PEVK region in the I-band. Results from cardiac muscle titin in which the PEVK region is greatly truncated were consistent with this conclusion.

The experimental values of contour length of the two chains are in most cases close to the values predicted from sequence information, though with uncertainty regarding the complement of isoforms of different length (Table 7 and Fig. 7). The values for total contour length suggest that the isoforms present were at the low end of the predicted range, ~1700 nm between the antibody pair T12-AB5 compared with the prediction of 1800–1900 nm (Table 2) from the sequence for the soleus muscle titin isoform. The range of contour lengths, especially for the whole skeletal muscle titin data set, is fairly broad (standard deviation ~ 120 nm). High-resolution sodium dodecyl sulfate (SDS) gel electrophoresis of titin prepared from rabbit longissimus dorsi muscle (Neagoe et al., 2003) suggests that the molecular mass distribution of the whole molecule is also broad (~200 kDa).

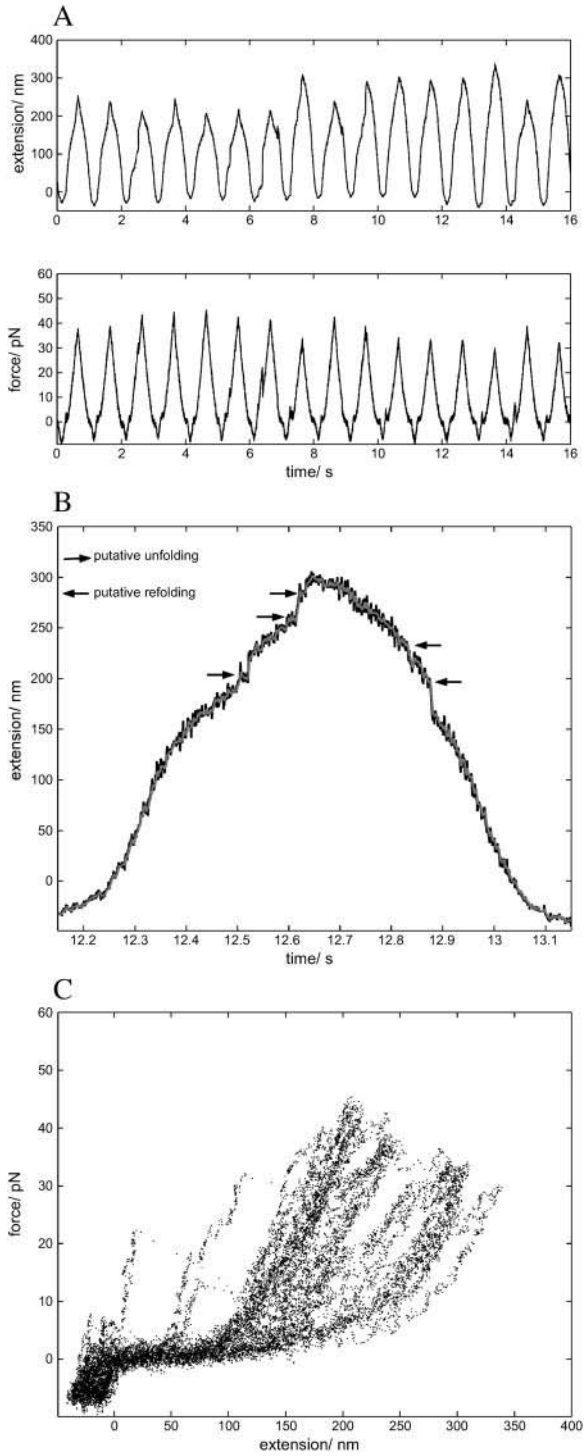

FIGURE 11 Triangle wave stretches of the native PEVK region (for long-lived tethers). (*A*) Force and extension records of consecutive cycles exhibiting hysteresis between stretch and release. (*B*) Expansion of a single stretch-release cycle (*solid*) of the data in *A*, with the output from the Chung-Kennedy filter (*shaded*). Detected step events are marked with arrows. (*C*) Overlaid force-extension relations for the stretch-release cycles of *A*.

The effect this will have on total contour length depends on the relative differential splicing of Ig domains to residues in the PEVK region (Freiburg et al., 2000); if the difference in molecular mass were due solely to differences in Ig expression number, the expected width of the contour length range would be ~90 nm, assuming ~10 kDa for each domain with a contour length of 4.4 nm. If the molecular mass difference were due solely to differences in numbers of residues in the PEVK region the expected width of the contour length range would be ~690 nm. The observed width of the distribution, taken as three standard deviations is 360 nm, midway between the two extremes.

However, it is also possible that errors in the fitting procedure could increase the apparent range of values of contour length. The standard deviations of the components of the two chain fits are at least twice as high as the single chain fits to the same data, possibly indicating an inverse correlation between the contour lengths of the two components but perhaps more likely indicating the error introduced by the fitting procedure.

Using a heterogeneous population of titin isomers, even if prepared from the same muscle, is potentially a weakness in the technique, and the reverse-engineering approach utilizing concatemers of the same or similar Ig domains, or with constructs of the PEVK or N2-B region whose sequences are known (Watanabe et al., 2002; Li et al., 2002), has some clear advantages (though with the obvious disadvantage that the whole in vivo region is not measured).

The contour lengths and persistence lengths determined for chain I and chain II using the different antibody pairs are fairly consistent. The most notable inconsistency in the results lies in the parameters for the whole molecule: the value of 723 nm determined for the contour length of chain I (putatively PEVK), differs significantly from the value of 507–553 nm obtained for the I-band and the PEVK region itself. Further, the value of L_p for the PEVK region for the whole molecule is lower (0.50 nm) than from the other measurements. The possibility that there is an additional elastic structure in the whole molecule with a low value of L_p is apparently inconsistent with the results from other antibody pairs. However, although not statistically significant at a confidence level of $P < 0.01$, there was an indication for an improvement in fit by including a small enthalpic factor for the whole skeletal muscle titin data set, which would be manifest as an artifactually lower persistence length if modeled as a pure entropic worm-like chain. This might account for the discrepancy in L_p and may also indicate that a pure entropic model for the elasticity of the whole titin molecule is not the complete picture. The tendency for a poor fit at low force in some (but not all) of the records might also be due to a partial long-range ordering (further discussed below). In general, it would not be surprising in such a complex molecule if there were nonentropic intrachain interactions that became apparent for the whole molecule but not for restricted regions, but

a further increase in accuracy and reduction in noise would be necessary to take the matter further.

Our values of L_c for the whole molecule divide contour length between chain I and chain II in much the same proportion as in the previous optical tweezers study of whole titin (Tskhovrebova et al., 1997), but the values of L_p are considerably different: 0.5 nm and 3.0 nm for chain I and chain II, respectively, reported here; 0.15 and 4.6 nm in the previous study. We took pains to avoid multiple attachments, which may have been present in the previous study (Tskhovrebova et al., 1997), and our value for L_p for chain I is appropriately higher than the previous value. However, if this is the right explanation, our value of L_p for chain II of 3.0 nm is inconsistently lower than the value of 4.6 nm found by Tskhovrebova et al. (1997). This suggests that the low value for L_p for chain I in the previous study may have resulted from an inaccuracy in the force-extension relation. The method used was a single bead assay that required a problematic geometrical correction at small extensions. Simulations show that an artifactually low value of L_p for chain I can result systematically from misalignments between the laser beam and the position of binding of the molecule where it is tethered to the coverslip (our unpublished observations).

Finally, all our values for L_p for the PEVK region or construct lie within the range of recent values from other studies (Li et al., 2001, 2002; Watanabe et al., 2002). Our value for L_p of 1.8 nm for the PEVK construct also lies within the range found by others; the difference with respect to the native PEVK region may simply be due to the partial nature of the PEVK construct. The result suggests that the native PEVK region may be heterogeneous in terms of serial stiffness elements, and the higher persistence length of the construct implies a greater proportion of stiffer elements compared to the native region. In the native PEVK region of the soleus muscle titin isoform, the presence of 28-mer repeats (Ma et al., 2001) accounts for 50–55% of the total sequence, compared with 35% in the construct. The difference in L_p would then follow if the 28-mer repeats were to be intrinsically less stiff than the rest of the molecule. The comparatively large scatter in the PEVK construct data may reflect the variability reported by Li et al. and Watanabe et al.

There is also an anomaly in the occurrence of hysteresis: hysteresis was present with both the construct and native PEVK regions to a much greater extent than for whole or I-band titin, which include the PEVK region. It is conceivable that the hysteresis in the case of the two PEVK experiments resulted from a PEVK-bead interaction, with hysteresis arising from a desorption-absorption effect. However, the very different methods of tether-bead conjugation and bead blocking in the native and construct PEVK elements argue against this, though not conclusively. Monte Carlo simulations based on a broad range of kinetic parameters (Supplementary Material) suggest that there may well be a masking effect of PEVK hysteresis due principally to the dominant compliance of the tandem Ig region of the whole titin molecule at the low forces over which putative stress relaxation in the PEVK region occurs, though the absence of accurate kinetic data for these models makes prediction imprecise. The alternative explanation, that there is a PEVK-Ig domain interaction that is disrupted by conjugation to beads across the PEVK region, would require the interaction to cause the denaturation of the PEVK structure, and this also seems far-fetched.

There remains a major discrepancy between our value of L_p for the Ig/Fn domains of ~3 nm, and the 4–14-fold higher values from myofibril and from light scattering and EM studies (Higuchi et al., 1993; Tskhovrebova and Trinick, 2001; Linke et al., 1998b), for which there seems to be no clear explanation. As noted above, there is a suggestion that our value of L_p for chain II is an underestimate, but probably not on the scale of the discrepancy.

There is an apparent anomaly in the results from short-lived tethers, which stems from the observation that both components in two chain fits vary in contour length (Fig. 4). If chain I does indeed correspond to the PEVK region, it might be expected that this component would either be completely present or absent depending on which side of the PEVK region the bead is bound, since the region would present a smaller target than the rest of the molecule. Several additional hypotheses might explain this result: some fraction of chain I might lie outside the PEVK region (this cannot be excluded within the errors of the results); the PEVK region might have a comparatively open structure; its high charge might make it a more likely target for binding; there is an anomaly in the fitting procedure. A more detailed study would be necessary to distinguish between the different relationships between contour lengths implied by these hypotheses.

Ionic strength and temperature effects

After the initial stretch-release cycles that evoked stepwise lengthening (and shortening), the force-extension relation of both native and construct PEVK settled down to a steady state free from overt lengthening steps, though still displaying a small amount of hysteresis. The force-extension relation then showed a marked dependence on ionic strength, with L_p having a dynamic range of 0.4–2.7 nm for ionic strengths of 15–300 mM (Fig. 8). At a given force, this implies that the higher the ionic strength, the lower is the stiffness. The PEVK region is highly charged (Fig. 12), so it is reasonable to suppose that screening of electrostatic charge is responsible for this effect. Coupled with the observed step-like stress relaxation of the PEVK construct, this suggests that the PEVK region might have an underlying microstructure, possibly of an electrostatic origin, whose mechanical properties cannot be attributed to a simple random coil. If the structure were held together by chain-chain interactions, perhaps by transient contacts, then raised ionic strength would result in weakening of these bonds, and a less stiff

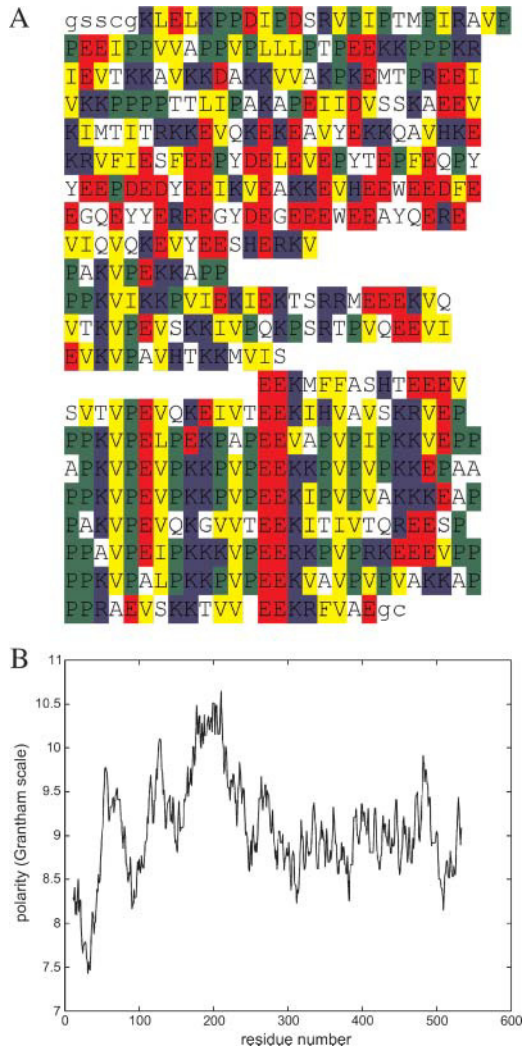

FIGURE 12 (*A*) Sequence alignment of PEVK construct (N-terminus at the top), using color coding of yellow equals hydrophobic, green equals non-α-helical, red equals negatively charged, and blue equals positively charged. (*B*) Variation of polarity across length (N-terminus defined as zero) of the PEVK construct using the Grantham polarity scale (Grantham, 1974) using a running window of size 21 convoluted with a symmetrical triangle function.

force opposing extension as observed, though it is not clear whether this would necessarily explain the larger value of L_p. Li et al. (2001) suggest that proline residues may exist as a mixture of *cis* and *trans*, but that under experimental stretch conditions the *cis-trans* transition is unlikely, thereby locking the PEVK into distinct conformations. Whether this could account for such a large range in the persistence length is again not obvious, nor is the effect of ionic strength.

For the PEVK construct, L_p was found to fall with increasing temperature, implying a tendency to shorten. This is consistent with rubber-like as opposed to steel-like behavior, i.e., an entropic basis to elasticity as opposed to enthalpic, but as noted earlier the amount of increase of force is greater than predicted by a random chain formula. Polyelectrolyte theory makes no unique prediction as to the direction of change of total persistence length with added salt, since this is the sum of the neutral-chain persistence length with the electrostatic persistence length, and the latter can be either positive or negative depending on whether the ionic strength is less or greater than a critical value at which so-called polyelectrolyte condensation occurs (Ariel and Andelman, 2003).

The observed changes in persistence and contour length with temperature suggest that the PEVK construct has a more compact conformation as temperature is increased. The fact that the value of L_c fell with increase of temperature is probably a result of the comparatively low maximal force that could be applied. A possible explanation can be found in the variation of Gibbs energy of hydration of the peptide as a function of temperature. At any temperature, the Gibbs energy of hydration per unit surface area is significantly less for polar residues than residues containing aliphatic or aromatic side chains (Privalov and Makhatadze, 1993), accounting for the usual distribution of polar residues on the outer water accessible surface of a compact peptide in water with nonpolar residues forming an inner hydrophobic core. The unfolding of a compact peptide involves hydrating the core nonpolar residues implying a loss in entropy. However, in a conventional folded protein the unfolding process involves the breaking of hydrogen bonds freeing the protein to adopt many more potential conformations thus implying a gain in entropy. In most instances this gain by far outweighs the loss due to core-residue hydration and the total Gibbs energy change for the unfolding transition decreases with temperature, implying the process is more favorable. The ratio of Gibbs energies of hydration for nonpolar compared to polar residues per unit surface area increases with temperature, the value at 50°C being roughly twice that at 5°C (Privalov and Makhatadze, 1993), suggesting that the change in Gibbs energy of hydration between the compact and the noncompact structures increases with temperature, i.e., favoring a more compact structure. If the PEVK region contains compact structures that are not held together by inner-core hydrogen bonds but rely on the hydrophobicity of the core alone (i.e., relatively loose compact structures) then structures of a greater compactness will be favored with increasing temperature. Current data on the structure of the PEVK are in agreement with this interpretation (Ma et al., 2001).

Stepwise lengthening

Stepwise lengthening was observed for the PEVK construct and for the native PEVK region. In some cases, the PEVK construct showed two types of lengthening during triangle wave stretches, involving also a statistically significant change in persistence length: 1), starting with an L_c of ~10 nm and L_p of 0.05–0.2 nm, early lengthening took place in a few steps until L_c was ~100 nm and L_p was constant at

~0.3–1.8 nm (depending on ionic strength); and 2), late lengthening at higher forces in which L_p was constant at 0.3–1.8 nm, and the lengthening steps were multiples of 11–12 nm. Shortening steps of ~11–12 nm were also observed during the release. In other cases, only the second, late type of lengthening was observed. For the native PEVK region it was not possible to quantitate the steps in the same way, but the range of contour lengths suggests that the maximal number of steps was ~30.

Fig. 12 *A* shows a sequence alignment of the PEVK construct, with the variation of polarity across its length shown in Fig. 12 *B*. There are seven modules, each 27–28 residues long and putatively associated with the polyproline-II triple-helical structural motif (Ma et al., 2001), that can be identified clearly from the alignment (there is one less clear repeat, starting SVTVPEVQKE, so the maximal number is probably eight). Each module would have a predicted extended length of 10.2–10.6 nm. As the maximal number (seven) and size (11–12 nm) of the later lengthening events correlate so closely to the values for the polyproline structural modules, we tentatively equate the two. There is also a consistency between the maximal number of steps observed in the case of the native PEVK region, viz., ~30, and the number of polyproline modules in native titin, viz., ~40 in the soleus muscle isoform.

In attempting to explain the origin of the lengthening events, it is not immediately obvious whether the steps observed are unfolding events per se or whether they are due to the desorption of structures bound to the surface of a bead, and we shall consider both possibilities. In the case of the early lengthening steps, the value of L_p is low, suggesting that perhaps half of the structure either unfolds or desorbs to a random coil configuration with little hindered movement. When the late 11–12-nm lengthening steps take place, the value of L_p rises progressively, indicating that each module, once it pulls away from the molecule or surface, has a locally more rigid structure. Desorption would require that the structural modules involved in stepwise lengthening are bound directly to the bead (or beads) and that one residue (or a small group of residues) of the 27–28 residue repeat is bound more strongly than the other residues, so that an applied force causes the 27–28 residue module under most stress to unzip from the surface.

The explanation of stepwise lengthening in terms of unfolding, or more precisely intramolecular lengthening, has two major possibilities: 1), *cis-trans* isomerization of proline residues; and 2), unfolding, either in the sense of unzipping of pairs of extended parallel chains or of unfolding of globular microdomains. The fact that ionic strength appears to be largely irrelevant to stepping, whereas increasing the temperature increases the stepping likelihood, but not the size of the step, suggests that electrostatic interactions cannot be the principle source of stability for such domains.

Polyproline chains have two distinct secondary structure states denoted as type I (PI) and type II (PII) polyproline helices, such that an isomerization change of proline residues from *cis* to *trans* (the lower energy state) converts PI to PII. This leads potentially to different total contour and persistence lengths (Tonelli, 1974). The energy difference between the two states is of the order of 1–2 kcal mol^{-1} (Wuthrich and Grathwohl, 1974), though the activation barrier for the *cis-trans* transition is significantly higher at 21 kcal mol^{-1} (Pauling, 1960) with a gain in length of ~0.1 nm. Equating this length gain to the width of the activation potential and using a value of 2×10^{-3} s^{-1} for the spontaneous isomerization rate (Schimmel and Florey, 1968) allows an estimation of the most likely force at which the transition occurs, using the model of Evans and Ritchie (1997). For the PEVK construct, there are 97 prolines (nine within each of the (27–28)-mer repeats), and for the range of loading used we estimate most likely transition forces of between 25 and 120 pN within the practical force range of the laser trap. However, to increase the total contour length by only 1 nm requires 10 such isomerizations, and we calculate that the likelihood of this alone occurring within a single stretch release cycles is less than 1 in 10^4, so it seems highly unlikely that this could account for the observed contour length changes in excess of 10 nm, a point that has also been argued previously as an explanation against proline isomerization accounting for a large distribution in values of persistence lengths (Watanabe et al., 2002).

It is more likely that the steps arise from a structural detachment of equal peptide units away from the bulk of the molecule and adopting a more open configuration. This could occur by the unzipping of pairs of parallel chains held together by electrostatic forces or from unfolding of a domain whose structure is not stabilized by intramolecular electrostatic interactions alone. The observation that the probability of stepping showed no significant dependence on ionic strength suggests the former explanation is unlikely unless the bonds are shielded from the solution. A potential candidate is clearly the polyproline-II helical motif. If it is modeled crudely as a sphere of diameter D composed of 28 smaller nondeformable spheres of diameter d, then $D \approx (28)^{1/3}d$. Thus, if lengthening is due to the small spheres being stretched out to a string-of-beads conformation, the change in contour length is given by $\Delta L_c = 28d - D \approx d(28 - (28)^{1/3})$. If $d \approx 0.4$ nm (the α-carbon spacing), this gives $\Delta L_c \approx$ 10 nm, close to the first-order peak observed for contour length change. This calculation also suggests that $D \approx 1.2$ nm, so that all seven folded modules will have a total contour length of ~8.5 nm. This would be consistent with the value of L_c of ~10 nm observed before the earliest step, provided the residues outside the repeated modules are tightly packed.

Recent evidence from stretches of soleus muscle myofibrils (Trombitas et al., 2003) has suggested that stress relaxation cannot be accounted for by Ig domain unfolding alone but that it can be better modeled with the addition of rupturing bonds in the PEVK region. These may well be the same stepwise lengthening we observe in this study.

However, they speculate that their rupturing bonds are electrostatic in nature, but since we observe stepwise lengthening at relatively high ionic strengths (300 mM), high enough to screen weak electrostatic interactions, this is unlikely to be the case and may suggest a more hydrophobic origin in bond formation.

Although it is possible to account for the observed stepwise lengthening in terms of unfolding, there is no compelling evidence to prefer it in to an explanation based on stepwise desorption of the repeats from the bead surface. Stepwise lengthening has not been observed in analogous AFM experiments with a shorter construct of cardiac titin PEVK (Li et al., 2001, 2002; Watanabe et al., 2002); though differential splicing results in the removal of over 90% of the ~28-mer polyproline repeats of this PEVK isoform compared to the soleus muscle PEVK (Supplementary Material; Greaser, 2001). However, stepwise lengthening was not observed with the PEVK construct (PEVK1) used here in an AFM stretch experiment (M. Rief, Ludwig Maximillians Universität, personal communication, 2003) or with an AFM single molecule mechanical study on a different skeletal muscle PEVK construct (Labeit et al., 2003), which may indicate that the surface charge of the bead or substrate, a major difference between the AFM and optical tweezers experiments, is a relevant factor and may favor an explanation for stepwise lengthening based on desorption. Since the putative stress relaxation in the PEVK region we observe in this study occurs at comparatively low forces (in the region of ~10–50 pN), it is not clear that a typical silicon nitride cantilever force transducer as used in AFM force spectroscopy would have the resolution to resolve steps in extension in the range 5–10 nm at such a low force, when the force resolution is inferior (typical rms noise 5–10 pN for a 1-kHz measurement bandwidth), compared to our (relatively) low stiffness force transducer (rms noise 0.5–1.0 pN on the unfiltered signal, 1-kHz bandwidth), a point consistent with the critique of Watanabe et al. (2002) concerning the resolution limitations of their own AFM. Further investigation of the different aspects of titin hysteresis found in this and other reports is clearly desirable.

A further complication is that there is a wearing-out effect, by which refolding or reabsorption rapidly diminishes with the number of stretch-release cycles, although here this phenomenon, also observed with unfolding of Ig domains (Kellermayer et al., 1997), is largely consistent with the establishment of steady-state conditions for the folded and unfolded states at a given rate of stretch. Molecular fatigue was also observed by Kellermayer et al. (2001), with some evidence that this might be due to intrachain rupture, possibly involving breaking of cross-links in the PEVK region. However, Kellermeyer et al. speculate that these intrachain bonds might be electrostatic in nature; as noted above, since we still observed stepwise lengthening at 300 mM ionic strength, this explanation seems unlikely.

Implications for mechanical properties of the skeletal muscle sarcomere

The parameters derived from the polymer fits of stretches on the I-band region of single titin molecules obtained here can be used to predict the shape of the force-extension curve with the additional contribution of Ig domain unfolding under steady-state conditions (Supplementary Material). The calculated force-extension relation is shown in Fig. 13 *A*. Unfolding of proximal Ig's appears to be much more relevant than unfolding of distal Ig's in the physiological force range (we estimate from the above model that a ~30% increase in sarcomere rest length, equivalent to a high force physiological stretch, equates to a titin mean extension of ~390 nm in each half-sarcomere; the persistence and contour length parameters obtained in this study, and the Ig unfolding parameters of other studies as indicated, give the force per titin molecule at an extension of 390 nm to be ~4 pN,

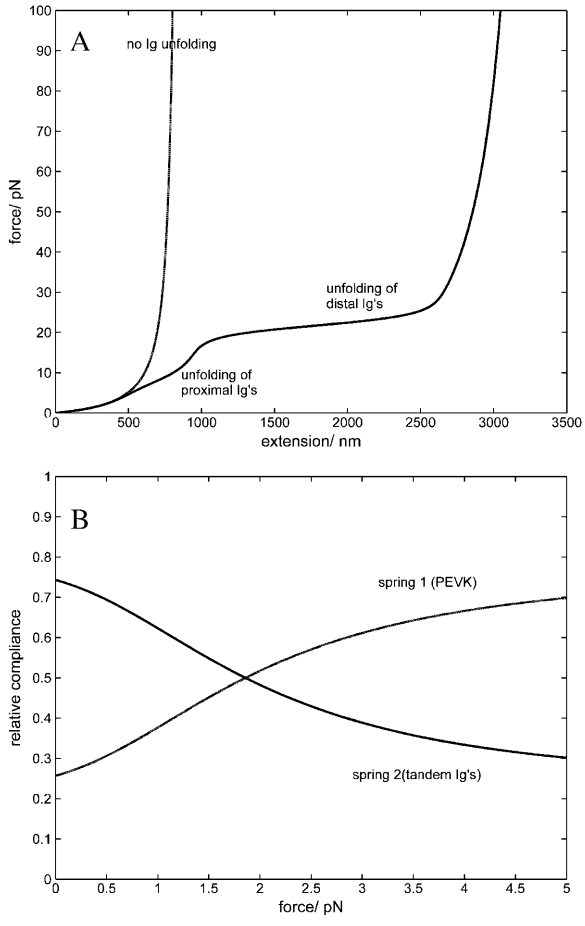

FIGURE 13 (*A*) Theoretical force-extension relation using parameters derived from the polymer fits of stretches on the I-band region of skeletal muscle titin, including the effect of Ig domain unfolding under of steady-state conditions (*solid line*); no Ig unfolding (*dotted line*). (*B*) Variation of the relative compliance of chain I (associated with the PEVK region, *dotted line*) and chain II (associated with tandem Ig's, *solid line*) with force (in the range of 0–5 pN) for the I-band region.

implying a force range of 0–4 pN per titin molecule), which can be readily seen by comparing P_{prox} with P_{dist} at 4 pN, viz., 0.14 and 3×10^{-6}, respectively. The relative compliance of each entropic element is shown as a function of force in Fig. 13 *B*. The long persistence length element (associated with the tandem-Ig's) contributes the bulk of the total compliance in the low force range, but as force is increased the tandem-Ig elasticity stiffens relative to the PEVK component, becoming equal in stiffness to it at 2 pN, and at the end of the force range ~3/4 of the total compliance is due to the PEVK component.

The physiological role, if any, of the stress relaxation of the PEVK region remains unclear. The stability of the putative PEVK modules is much lower than the Ig domains, as reflected in the lower unfolding force, and it could be that the PEVK modules act as shock absorbers in much the same way as has been speculated for Ig domains (Tskhovrebova et al., 1997) but for lower forces. There is also some evidence that the PEVK region interacts with thin filaments to provide a source of viscous drag (Linke et al., 1997; Opitz et al., 2003), though there is evidence that only the PEVK region common to cardiac titin will bind F-actin (Yamasaki et al., 2001). PEVK stress relaxation might affect the strength of this interaction and be a mechanism allowing the switching between low and high viscous-drag states.

SUPPLEMENTARY MATERIAL

An online supplement to this article can be found by visiting BJ Online at http://www.biophysj.org.

We thank Professor John Trinick for the antibodies AB5, anti-I84–86, and N2-A (the latter two were originally produced in the laboratory of Dr. Siegfried Labeit) and also for a gift of cardiac muscle titin. We are grateful to Dr. David Smith for software.

This work was supported by funds from the Medical Research Council and the Human Frontier Science Programme to R.M.S. and from the Deutsche Forschungsgemeinschaft and Medical Research Council to M.G. M.L. was supported by a research studentship from the Biotechnology and Biological Sciences Research Council.

REFERENCES

Ariel, G., and Andelman, D. 2003. Persistence length of a strongly charged rodlike polyelectrolyte in the presence of salt. *Phys. Rev. E*. 67:011805.

Carrion-Vazquez, M., A. F. Oberhauser, S. B. Fowler, P. E. Marszalek, S. E. Broedel, and J. Clarke. 1999. Mechanical and chemical unfolding of a single protein: a comparison. *Proc. Natl. Acad. Sci. USA*. 96: 3694–3699.

Chung, S. H., and R. A. Kennedy. 1991. Forward-backward non-linear filtering technique for extracting small biological signals from noise. *J. Neurosci. Methods*. 40:71–86.

Evans, E., and K. Ritchie. 1997. Dynamic strength of molecular adhesion bonds. *Biophys. J*. 72:1541–1555.

Evans, E., and K. Ritchie. 1999. Strength of a weak bond connecting flexible polymer chains. *Biophys. J*. 76:2439–2447.

Florey, P. J. 1969. Statistical Mechanics of Chain Molecules. Interscience Publishers, New York.

Fraternali, F., and Pastore, A. 1999. Modularity and homology: modeling of the type II module family from titin. *J. Mol. Biol*. 290:581–593.

Freiburg, A., K. Trombitas, W. Hell, O. Cazorla, F. Fougerousse, T. Centner, B. Kolmerer, C. Witt, J. S. Beckmann, C. C. Gregorio, H. Granzier, and S. Labeit. 2000. Series of exon-skipping events in the elastic spring region of titin as the structural basis for myofibrillar elastic diversity. *Circ. Res*. 86:1114–1121.

Fürst, D. O., M. Osborn, R. Nave, and K. Weber. 1988. The organization of titin filaments in the half-sarcomere revealed by monoclonal antibodies in immunoelectron microscopy: a map of ten nonrepetitive epitopes starting at the Z line extends close to the M line. *J. Cell Biol*. 106:1563–1572.

Gautel, M., E. Lehtonen, and F. Pietruschka. 1996a. Assembly of the cardiac I-band region of titin/connectin: expression of the cardiac-specific regions and their relation to the elastic segments. *J. Muscle Res. Cell Motil*. 17:449–461.

Gautel, M., and D. Goulding. 1996. A molecular map of titin/connectin elasticity reveals two different mechanisms acting in series. *FEBS Lett*. 385:11–14.

Gautel, M., D. Goulding, B. Bullard, K. Weber, and D. O. Fürst. 1996b. The central Z-disk region of titin is assembled from a novel repeat in variable copy numbers. *J. Cell Sci*. 109:2747–2754.

Goll, C. M., A. Pastore, and M. Nilges. 1998. The three-dimensional structure of a type I module from titin: a prototype of intracellular fibronectin type III domains. *Structure*. 6:1291–1302.

Grantham, R. 1974. Amino acid difference formula to help explain protein evolution. *Science*. 185:862–864.

Granzier, H., M. Helmes, and K. Trombitas. 1996. Nonuniform elasticity of titin in cardiac myocytes: a study using immunoelectron microscopy and cellular mechanics. *Biophys. J*. 70:430–442.

Granzier, H. L., and T. C. Irving. 1995. Passive tension in cardiac muscle: contribution of collagen, titin, microtubules, and intermediate filaments. *Biophys. J*. 68:1027–1044.

Greaser, M. L. 2001. Identification of new repeating motifs in titin. *Proteins*. 43:145–149.

Higuchi, H., Y. Nakauchi, K. Maruyama, and S. Fujime. 1993. Characterization of beta-connectin (titin 2) from striated muscle by dynamic light scattering. *Biophys. J*. 65:1906–1915.

Kellermayer, M. S., S. B. Smith, C. Bustamante, and H. L. Granzier. 1998. Complete unfolding of the titin molecule under external force. *J. Struct. Biol*. 122:197–205.

Kellermayer, M. S., S. B. Smith, C. Bustamante, and H. L. Granzier. 2001. Mechanical fatigue in repetitively stretched single molecules of titin. *Biophys. J*. 80:852–863.

Kellermayer, M. S., S. B. Smith, H. L. Granzier, and C. Bustamante. 1997. Folding-unfolding transitions in single titin molecules characterized with laser-tweezers. *Science*. 276:1112–1116.

Kuo, S. C. 1998. A simple assay for local heating by optical tweezers. *Meth. Cell Biol*. 55:43–45.

Labeit, S., M. Gautel, A. Lakey, and J. Trinick. 1992. Towards a molecular understanding of titin. *EMBO J*. 11:1711–1716.

Labeit, S., and B. Kolmerer. 1995. Titins: giant proteins in charge of muscle ultrastructure and elasticity. *Science*. 270:293–296.

Labeit, D., K. Watanabe, C. Witt, H. Fujita, Y. Wu, S. Lahmers, T. Funck, S. Labeit, and H. Granzier. 2003. Calcium-dependent molecular spring elements in the giant protein titin. *Proc. Natl. Acad. Sci. USA*. 100: 13716–13721.

Leake, M. C., D. Wilson, B. Bullard, and R. M. Simmons. 2003. The elasticity of single kettin molecules using a two-bead laser-tweezers assay. *FEBS Lett*. 535:55–60.

Li, H., W. A. Linke, A. F. Oberhauser, M. Carrion-Vazquez, J. G. Kerkvliet, H. Lu, P. E. Marszalek, and J. M. Fernandez. 2002. Reverse engineering of the giant muscle protein titin. *Nature*. 418:998–1002.

Li, H., A. F. Oberhauser, S. D. Redick, M. Carrion-Vazquez, H. P. Erickson, and J. M. Fernandez. 2001. Multiple conformations of PEVK proteins detected by single-molecule techniques. *Proc. Natl. Acad. Sci. USA*. 98:10682–10686.

Linke, W. A., M. Ivemeyer, S. Labeit, H. Hinssen, J. C. Ruegg, and M. Gautel. 1997. Actin-titin interaction in cardiac myofibrils: probing a physiological role. *Biophys. J.* 73:905–919.

Linke, W. A., M. Ivemeyer, P. Mundel, M. R. Stockmeier, and B. Kolmerer. 1998a. Nature of PEVK-titin elasticity in skeletal muscle. *Proc. Natl. Acad. Sci. USA.* 95:8052–8057.

Linke, W. A., M. Ivemeyer, N. Olivieri, B. Kolmerer, J. C. Ruegg, and S. Labeit. 1996. Towards a molecular understanding of the elasticity of titin. *J. Mol. Biol.* 261:62–71.

Linke, W. A., M. R. Stockmeier, M. Ivemeyer, H. Hosser, and P. Mundel. 1998b. Characterizing titin's I-band Ig domain region as an entropic spring. *J. Cell Sci.* 111:1567–1574.

Ma, K., L. S. Kan, and K. Wang. 2001. Polyproline II helix is a key structural motif of the elastic PEVK segment of titin. *Biochemistry.* 40:3427–3438.

Marko, J. F., and E. Siggia. 1995. Stretching DNA. *Macromolecules.* 28:209–212.

Minajeva, A., M. Kulke, J. M. Fernandez, and W. A. Linke. 2001. Unfolding of titin domains explains the viscoelastic behavior of skeletal myofibrils. *Biophys. J.* 80:1442–1451.

Nave, R., D. O. Fürst, and K. Weber. 1989. Visualization of the polarity of isolated titin molecules; a single globular head on a long thin rod as the M-band anchoring domain? *J. Cell Biol.* 109:2177–2188.

Neagoe, C., C. A. Opitz, I. Makarenko, and W. A. Linke. 2003. Gigantic variety: expression patterns of titin isoforms in striated muscles and consequences for myofibrillar passive stiffness. *J. Muscle Res. Cell Motil.* 24:175–189.

Nelder, J. A., and R. Mead. 1965. A simplex method for function minimization. *Comput. J.* 7:308–313.

Opitz, C. A., M. Kulke, M. C. Leake, C. Neagoe, H. Hinssen, R. J. Hajjar, and W. A. Linke. 2003. Damped elastic recoil of the titin spring in myofibrils of human myocardium. *Proc. Natl. Acad. Sci. USA.* 100:12688–12693.

Pauling, L. 1960. The Nature of the Chemical Bond, 3rd ed. Cornell University Press, Ithaca, NY.

Peckham, M., P. Young, and M. Gautel. 1997. Constitutive and variable regions of Z-disk titin/connectin in myofibril formation: a dominant-negative screen. *Cell Struct. Funct.* 22:95–101.

Pfuhl, M., M. Gautel, A. S. Politou, C. Joseph, and A. Pastore. 1995. Secondary structure determination by NMR spectroscopy of an immunoglobulin-like domain from the giant muscle protein titin. *J. Biomol. NMR.* 6:48–58.

Privalov, P. L., and G. I. Makhatadze. 1993. Contribution of hydration to protein folding thermodynamics. II. The entropy and Gibbs energy of hydration. *J. Mol. Biol.* 232:660–679.

Rief, M., M. Gautel, F. Oesterhelt, J. M. Fernandez, and H. E. Gaub. 1997. Reversible unfolding of individual titin immunoglobulin domains by AFM. *Science.* 276:1109–1112.

Rief, M., M. Gautel, A. Schemmel, and H. E. Gaub. 1998. The mechanical stability of immunoglobulin and fibronectin III domains in the muscle protein titin measured by atomic force microscopy. *Biophys. J.* 75:3008–3014.

Schimmel, P. R., and P. J. Flory. 1968. Conformational energies and configurational statistics of copolypeptides containing L-proline. *J. Mol. Biol.* 34:105–120.

Schwesinger, F., R. Ros, T. Strunz, D. Anselmetti, H. J. Guntherodt, A. Honegger, L. Jermutus, L. Tiefenauer, and A. Pluckthun. 2000. Unbinding forces of single antibody-antigen complexes correlate with their thermal dissociation rates. *Proc. Natl. Acad. Sci. USA.* 97:9972–9977.

Simmons, R. M., J. T. Finer, S. Chu, and J. A. Spudich. 1996. Quantitative measurements of force and displacement using an optical trap. *Biophys. J.* 70:1813–1822.

Svoboda, K., and S. M. Block. 1994. Biological applications of optical forces. *Annu. Rev. Biophys. Biomol. Struct.* 23:247–285.

Tonelli, A. E. 1974. Conformational characteristics of polypeptides containing isolated L-proline residues with cis peptide bonds. *J. Mol. Biol.* 86:627–635.

Trinick, J., P. Knight, and A. Whiting. 1984. Purification and properties of native titin. *J. Mol. Biol.* 180:331–356.

Trombitas, K., P. H. Baatsen, M. S. Kellermayer, and G. H. Pollack. 1991. Nature and origin of gap filaments in striated muscle. *J. Cell Sci.* 100:809–814.

Trombitas, K., M. Greaser, G. French, and H. Granzier. 1998. PEVK extension of human soleus muscle titin revealed by immunolabeling with the anti-titin antibody 9D10. *J. Struct. Biol.* 122:188–196.

Trombitas, K., G. H. Pollack, J. Wright, and K. Wang. 1993. Elastic properties of titin filaments demonstrated using a ''freeze-break'' technique. *Cell Motil. Cytoskeleton.* 24:274–283.

Trombitas, K., Y. Wu, M. McNabb, M. Greaser, M. S. Kellermayer, S. Labeit, and H. Granzier. 2003. Molecular basis of passive stress relaxation in human soleus fibers: assessment of the role of immunoglobulin-like domain unfolding. *Biophys. J.* 85:3142–3153.

Tskhovrebova, L., and J. Trinick. 1997. Direct visualization of extensibility in isolated titin molecules. *J. Mol. Biol.* 265:100–106.

Tskhovrebova, L., and J. Trinick. 2000. Extensibility in the titin molecule and its relation to muscle elasticity. *Adv. Exp. Med. Biol.* 481:163–178.

Tskhovrebova, L., and J. Trinick. 2001. Flexibility and extensibility in the titin molecule: analysis of electron microscope data. and its relation to muscle elasticity. *J. Mol. Biol.* 301:755–771.

Tskhovrebova, L., and J. Trinick. 2002. Role of titin in vertebrate striated muscle. *Phil. Trans. R. Soc. Lond. B.* 357:199–206.

Tskhovrebova, L., J. Trinick, J. A. Sleep, and R. M. Simmons. 1997. Elasticity and unfolding of single molecules of the giant muscle protein titin. *Nature.* 387:308–312.

Wang, S. M., and M. L. Greaser. 1985. Immunocytochemical studies using a monoclonal antibody to bovine cardiac titin on intact and extracted myofibrils. *J. Muscle Res. Cell Motil.* 6:293–312.

Wang, K., J. McClure, and A. Tu. 1979. Titin: major myofibrillar components of striated muscle. *Proc. Natl. Acad. Sci. USA.* 76:3698–3702.

Watanabe, K., P. Nair, D. Labeit, M. S. Z. Kellermayer, M. Greaser, S. Labeit, and H. Granzier. 2002. Molecular mechanics of cardiac titin's PEVK and N2B spring elements. *J. Biol. Chem.* 277:11549–11558.

Whiting, A., J. Wardale, and J. Trinick. 1989. Does titin regulate the length of muscle thick filaments? *J. Mol. Biol.* 205:263–268.

Williams, P. M., S. B. Fowler, R. B. Best, J. L. Toca-Herrera, K. Scott, A. Steward, and J. Clarke. 2003. Hidden complexity in the mechanical properties of titin. *Nature.* 422:446–449.

Wuthrich, K., and C. Grathwohl. 1974. A novel approach for studies of the molecular conformations in flexible polypeptides. *FEBS Lett.* 43:337–340.

Yamasaki, R., M. Berri, Y. Wu, K. Trombitas, M. McNabb, M. S. Kellermayer, C. Witt, D. Labeit, S. Labeit, M. Greaser, and H. Granzier. 2001. Titin-actin interaction in mouse myocardium: passive tension modulation and its regulation by calcium/S100A1. *Biophys. J.* 81:2297–2313.

Young, P., C. Ferguson, S. Banuelos, and M. Gautel. 1998. Molecular structure of the sarcomeric Z-disk: two types of titin interactions lead to an asymmetrical sorting of alpha-actinin. *EMBO J.* 17:1614–1624.